



**Fenretinide treatment accelerates atherosclerosis development in apoE-deficient mice in spite of beneficial metabolic effects**

Journal:	<i>British Journal of Pharmacology</i>
Manuscript ID	2019-BJP-0410-RP
Manuscript Type:	Research Paper
Date Submitted by the Author:	09-Apr-2019
Complete List of Authors:	<p>Busnelli, Marco; Università degli Studi di Milano, Dept. of Pharmacological Sciences            Manzini, Stefano; Università degli Studi di Milano, Dept. of Pharmacological Sciences            Bonacina, Fabrizia; Università degli Studi di Milano, Dept. of Pharmacological Sciences            Soldati, Sabina; Università degli Studi di Milano, Department of Veterinary Medicine            Barbieri, Silvia; IRCCS, Centro Cardiologico Monzino            Amadio, Patrizia; IRCCS, Centro Cardiologico Monzino            Sandrini, Leonardo; IRCCS, Centro Cardiologico Monzino            Arnaboldi, Francesca; Università degli Studi di Milano, Dept. of Biomedical Sciences for Health            Donetti, Elena; Università degli Studi di Milano, Dept. of Biomedical Sciences for Health            Laaksonen, Reijo; University of Tampere, Faculty of Medicine and Life Sciences            Paltrinieri, Saverio; Università degli Studi di Milano, Mouse and Animal Pathology Laboratory (MAPLab)            Scanziani, Eugenio; University of Milan, Animal Pathology, Hygiene and Public Health            Chiesa, Giulia; Università degli Studi di Milano, Department of Pharmacological Sciences</p>
Major area of pharmacology:	Atherosclerosis
Cross-cutting area:	Inflammation
Additional area(s):	Repurposing, Platelets/thrombocytes, Lipids, In vivo

SCHOLARONE™  
Manuscripts



## UNIVERSITÀ DEGLI STUDI DI MILANO

DIPARTIMENTO DI SCIENZE FARMACOLOGICHE  
E BIOMOLECOLARI - DiSFEB

*Direttore: Prof. Alberto Corsini*

April 9, 2019

Dear Prof. Ahluwalia,

we are submitting a manuscript entitled “Fenretinide treatment accelerates atherosclerosis development in apoE-deficient mice in spite of beneficial metabolic effects” by Busnelli et al., to be considered for publication in British Journal of Pharmacology.

Fenretinide, a synthetic retinoid derivative, is known for a much lower toxicity with respect to other retinoids, and is currently employed in several preclinical and clinical trials testing its ability to inhibit and treat different forms of cancer. In addition to this seemingly protective action, a plethora of beneficial metabolic effects have been described in the literature in both experimental models and patients, including an ameliorated glucose tolerance, lowered plasma lipid levels and a reduced fat mass deposition. All these evidences spurred us to investigate whether these beneficial effects would translate into a reduced atherosclerosis development in an animal model widely employed in this regard, the apolipoprotein E knockout mouse.

As yet untested, we could confirm that all evidences pointing towards beneficial metabolic effects were indeed confirmed also in this model: we found that fenretinide lowered the fat mass accumulation upon high-fat diet feeding, resulted into a lower basal glycemia and was able to reduce total cholesterol, phospholipids and triglycerides especially.

Very surprisingly, we found that atherosclerosis was indeed increased, and by a significant margin, in the treated group. With the aim of pinpoint the mechanism responsible for this result, we set out to deeply characterize our model, and we found how fenretinide exerts detrimental effects on erythrocytes as well as monocytes and leukocytes, effects partly stemming from an impaired myelopoiesis and erythropoiesis. To rule out possible model biases, we enrolled wild-type mice that were likewise treated. While it is not possible to evaluate atherosclerosis in such a model, we were able to identify the vast majority of



## UNIVERSITÀ DEGLI STUDI DI MILANO

DIPARTIMENTO DI SCIENZE FARMACOLOGICHE  
E BIOMOLECOLARI - DiSFeB

*Direttore: Prof. Alberto Corsini*

fenretinide treatment detrimental effects also in wild-type mice (enlarged spleen, leucocytosis). As already considered, Fenretinide is now being used to treat problematic patients with life-threatening conditions, and the adverse effects that we regard as detrimental are a minor concern in this kind of studies. However, our study raises a red flag, should fenretinide be repurposed as a treatment for more ordinary ailments, and/or for chronic treatments.

In summary, despite the beneficial metabolic effects that fenretinide reportedly exerts and that we confirmed, we demonstrate how fenretinide can negatively impact atherosclerosis development, and particular care must be taken should fenretinide enter everyday clinical practice.

We hope that this work will be considered of interest to the readers of British Journal of Pharmacology.

Sincerely yours,

## **Fenretinide treatment accelerates atherosclerosis development in apoE-deficient mice in spite of beneficial metabolic effects**

### Running Short Title:

### **Fenretinide worsens atherosclerosis development**

Marco Busnelli<sup>1\*</sup>, Stefano Manzini<sup>1\*</sup>, Fabrizia Bonacina<sup>1</sup>, Sabina Soldati<sup>2</sup>, Silvia Stella Barbieri<sup>3</sup>, Patrizia Amadio<sup>3</sup>, Leonardo Sandrini<sup>1,3</sup>, Francesca Arnaboldi<sup>4</sup>, Elena Donetti<sup>4</sup>, Reijo Laaksonen<sup>5</sup>, Saverio Paltrinieri<sup>2</sup>, Eugenio Scanziani<sup>2,6</sup>, Giulia Chiesa<sup>1</sup>.

<sup>1</sup>Department of Pharmacological and Biomolecular Sciences, Università degli Studi di Milano, Milano, Italy; <sup>2</sup>Department of Veterinary Medicine, Università degli Studi di Milano, Italy; <sup>3</sup>IRCCS, Centro Cardiologico Monzino IRCCS, Milano, Italy; <sup>4</sup>Department of Biomedical Sciences for Health, Università degli Studi di Milano, Italy; <sup>5</sup>Faculty of Medicine and Life Sciences, University of Tampere, Tampere, Finland; <sup>6</sup>Mouse and Animal Pathology Laboratory (MAPLab), Fondazione UniMi, Milano, Italy.

\* These authors equally contributed to this work.

Corresponding author: Giulia Chiesa, [giulia.chiesa@unimi.it](mailto:giulia.chiesa@unimi.it) and Marco Busnelli [marco.busnelli@unimi.it](mailto:marco.busnelli@unimi.it)



**Abbreviations**

apoE	Apolipoprotein E
Ctrl	Control, control group
EKO	apoE knockout
Fen	Fenretinide, fenretinide-treated group
HCT	Hematocrit
HGB	Hemoglobin concentration
MCH	Mean corpuscular hemoglobin
MCHC	Mean corpuscular hemoglobin concentration
MCV	Mean corpuscular volume
MP	Monocyte progenitors
PL	Phospholipids
PLT	Platelet
RBC	Red blood cells
TC	Total cholesterol
TG	Triglycerides
WAT	White adipose tissue
WBC	Total leukocytes, white blood cells
WT	Wild-type

## Abstract

**Background and Purpose:** Fenretinide, a synthetic retinoid derivative first investigated for cancer prevention and treatment, has been shown to ameliorate glucose tolerance and the plasma lipid profile, and to reduce body fat mass. These effects, together with its ability to inhibit ceramide synthesis, have suggested that fenretinide may display anti-atherosclerotic effects.

**Experimental Approach:** To this aim, 9-weeks-old apoE-knockout (EKO) female mice were fed for 12 weeks a Western diet, without (Control) or with (0.1% w/w) fenretinide. As a reference, wild-type (WT) mice were likewise treated. Growth and metabolic parameters were monitored throughout the study. Atherosclerosis development was evaluated in the aorta and at the aortic sinus. Blood and lymphoid organs were further characterized with thorough cytological/histological and immunocytofluorimetric analyses.

**Key Results:** Fenretinide treatment significantly lowered body weight, glucose levels and plasma levels of total cholesterol, triglycerides and phospholipids. In the liver, fenretinide remarkably reduced hepatic glycogenosis and steatosis driven by the Western diet. Treated spleens were abnormally enlarged, with severe follicular atrophy and massive extramedullary hematopoiesis. Severe renal hemosiderin deposition was observed in treated EKO. Treatment resulted in a threefold increase of total leukocytes (WT and EKO) and raised the activated/resting monocyte ratio in EKO. Finally, atherosclerosis development was markedly increased at the aortic arch ( $34.4 \pm 7.3\%$  vs  $26.1 \pm 5.8\%$ , +32%), thoracic ( $14.3 \pm 4.9\%$  vs  $4.9 \pm 2.1\%$ , +191%) and abdominal aorta ( $7.6 \pm 3.3\%$  vs  $3.3 \pm 1.8\%$ , +130%) of fenretinide-treated mice.

**Conclusions and Implications:** We provide the first evidence that, despite beneficial metabolic effects, fenretinide treatment may prove detrimental for atherosclerosis development.

## 1. Introduction

Fenretinide is a derivative of retinoic acid, widely investigated as chemopreventive option in different forms of cancer and as chemotherapeutic agent in both pediatric and adult malignancies (Cooper et al., 2017). Whereas retinoic acid and other related compounds preferentially accumulate in the liver, causing hepatic toxicity with prolonged exposure, fenretinide, together with its metabolites, is preferentially stored in fatty tissues, providing a safer profile to this molecule (Mody and Mcilroy, 2014).

The retinoid metabolism pathway is known to play an important role in body mass regulation and adipocyte biology (Zizola et al., 2010; Berry et al., 2012) and all-*trans*-retinoic acid, the most active metabolite of retinol, has been shown to positively affect obesity and glucose homeostasis (Berry and Noy, 2009). Fenretinide improves glucose response and modulates body fat mass, at least in part through modulation of retinoid homeostasis genes (Mcilroy et al., 2013; Mody and Mcilroy, 2014). Additionally, fenretinide prevents ceramide accumulation by inhibiting dihydroceramide desaturase, which catalyzes the final step of *de novo* ceramide synthesis (Bikman et al., 2012). Given the emerging role of ceramides in promoting insulin resistance and other obesity-induced metabolic alterations (Aburasayn et al., 2016; Petersen and Shulman, 2018), this mechanism may certainly account for the favourable metabolic effects of fenretinide treatment (Bikman et al., 2012; Mody and Mcilroy, 2014). Further, fenretinide administration to high fat fed mice has been shown to significantly reduce hepatic steatosis (Preitner et al., 2009; Koh et al., 2012) and to moderately lower plasma lipids, possibly by increasing liver fatty acid oxidation (Koh et al., 2012).

All these favourable metabolic effects exerted by fenretinide suggest that this drug may be protective against cardiovascular disease. In the present study, fenretinide was administered to apolipoprotein E (apoE)-deficient mice to investigate a possible beneficial effect of this drug on atherosclerosis development. Although fenretinide treatment favourably affected glucose and lipid metabolism, it unexpectedly worsened atherosclerosis, possibly through a dramatic increase of the immune/inflammatory response.

## 2. Methods

**2.1. Animals, diet and pharmacological treatment.** Procedures involving animals and their care were conducted in accordance with institutional guidelines that are in compliance with national (D.L. No. 26, March 4, 2014, G.U. No. 61 March 14, 2014) and international laws and policies (EEC Council Directive 2010/63, September 22, 2010: Guide for the Care and Use of Laboratory Animals, United States National Research Council, 2011). The experimental protocol was approved by the Italian Ministry of Health (Protocollo 428/2015-PR).

Fifty apoE knockout female mice (strain 002052), and twenty C57BL/6 wild type (strain 027) aged 8 weeks, were purchased from Charles River Laboratories (Calco, Italy) and housed at constant temperature and relative humidity. Scobis Uno, a vegetable bedding made of wood particles obtained from spruce, was used. After one week of acclimatization, mice were fed for 12 weeks a high-fat diet (adjusted calories 42% from fat, 0.2% cholesterol) without supplementation (Control), or supplemented with Fenretinide 0.1% w/w. Mice were housed 3-4 per cage.

**2.2. Blood and tissue harvesting.** At the end of the dietary treatment, mice were anesthetized with 2% isoflurane (Parolini et al., 2014), and blood was collected from a subset of mice, after 5 hours fast, for plasma lipid quantification, as described (Busnelli et al., 2017). In a second subset of unfasted mice, blood was collected for FACS (0.1% w/v EDTA) from the retroorbital plexus. For haematological analyses, blood was collected through cardiac puncture in 3.8% Na-citrate as described (Amadio et al., 2017a).

Blood was then removed by perfusion with PBS, and aorta was rapidly harvested as described (Parolini et al., 2017), longitudinally opened, pinned flat on a black wax surface in ice-cold PBS and photographed unstained for plaque quantification (see below).

Heart, liver, lungs, abdominal white adipose tissue (WAT), kidneys, skin, spleen and bone marrow were harvested. Liver and WAT were snap-frozen in liquid nitrogen for subsequent molecular analyses. All listed tissues were processed for subsequent histological or cytological analyses.

**2.3. Plasma measurements and glucose tolerance test.**

Plasma total cholesterol (TC), triglycerides (TG) and phospholipids (PL) were measured with enzymatic methods and lipid distribution among lipoproteins was analysed by FPLC (Marchesi et al., 2011).

For the glucose tolerance test, after 10 weeks of treatment mice were fasted for 5 hours and then injected with 2 g/Kg glucose via i.p. injection of 20% w/v sterile glucose solution in PBS. Glucose levels were determined as described previously (Lachance et al., 2013).

**2.4 Functional Fibrinogen** – Plasma fibrinogen was assayed by Clauss method according to manufacturer's instructions, as previously described (Amadio et al., 2017b). Briefly, plasma samples were diluted 1:10 in imidazole buffer (Imidazole 0.34%, NaCl 0.6%, Sodium citrate 0.15%, HCl 0.14%, Sodium azide 0.33%; pH 7.4). Two-hundred  $\mu$ L of each diluted plasma sample were pre-warmed at 37°C for 4 minutes and then clot formation was promoted by the addition of 100  $\mu$ L of liquid stable thrombin reagent (100 U/ml). The time taken for the clot to form is directly proportional to fibrinogen concentration present in the samples analyzed (Mackie et al., 2003).

## **2.5 Blood and bone marrow cytology.**

*2.5.1 Sampling.* At sacrifice, blood was collected from the heart and immediately placed in 0.5 mL tubes containing EDTA, filled at their maximum capacity. Anticoagulated blood was stored at room temperature and transported to the laboratory to be processed within 4 hours from sampling as described below.

Bone marrow was collected from the femur using a 24G syringe needle through the needle capillary technique: the femur was removed at necropsy and longitudinally split using a bone cutter and the needle was inserted in the bone marrow cavity. Once removed, the content of the needle was sprayed on a glass slide using a 1 mL syringe and the needle itself was rolled on the slide to smear either the material contained in the needle or the small drops of tissues remained in the outer surface of the needle.

*2.5.2 Hematology and Bone Marrow cytology.* Routine hematology was performed on whole blood collected in EDTA using a laser-based cell counter (Sysmex XT-2000iV) validated in mice (Mathers et al., 2008). Samples with evident clots were excluded from the haematological analysis. The following parameters were evaluated: erythrocyte number (RBC), hemoglobin concentration (HGB), hematocrit (HCT),

mean corpuscular volume (MCV), mean corpuscular hemoglobin (MCH), mean corpuscular hemoglobin concentration (MCHC), platelet number (PLT), number of total leukocytes (WBC), and of the different leukocyte populations: neutrophils, lymphocytes, monocytes, eosinophils, and basophils. The differential leucocyte counts provided by the instrument were verified through microscopic evaluation on May Grünwald Giemsa stained smears. During microscopic evaluation, particular attention was paid to the differentiation of mature (segmented) neutrophils and immature (band) neutrophils and to any possible morphological abnormality of erythrocytes, leukocytes and platelets.

Bone marrow smears were stained with May Grünwald Giemsa and a 500 nucleated-cell count was microscopically performed. The following parameters were recorded: myeloid:erythroid (M:E); number of cells belonging to the proliferative (P) pool (composed by blasts able to divide) or to the maturation (M) pool, in order to calculate, for each cell population, the P:M ratio and the percentage of precursors on the total number of cells belonging to each cell lineage (%EP = percentage of erythroid precursors and %MP = percentage of myeloid precursors); percentage of lymphocytes (%L) and plasma cells (%PL) on the total number of counted cells. Any possible abnormal morphology of cells of both proliferative and maturation pool was also recorded.

## **2.6. FACS Analyses.**

*2.6.1 Flow cytometry.* All fluorochrome-conjugated antibodies were used at 1:100 dilutions unless otherwise specified. Samples were acquired with Novocyte 3000 (ACEA Biosciences) and analysed with Novoexpress software.

*2.6.2 Blood immunophenotyping.* 50  $\mu$ L of blood were stained with the mix of fluorochrome-conjugated antibodies prepared in PBS containing, 2% FBS and 2 $\mu$ M EDTA (MACS buffer) at RT for 30 minutes in the dark. Following staining, red blood cells were lysed and fixed for 20 minutes at RT, washed twice and resuspended with MACS buffer and analysed immediately.

*2.6.3. Spleen and bone marrow cells immunophenotyping.* Spleens were weighed, then immune cells were isolated. A uniform cell suspension was prepared by the spleens through a 70  $\mu$ m cell strainer; after red blood cell lysis (Red Cell Blood Lysis Buffer), cells were spun down at 600 $\times$ g for 5 minutes suspended in MACS buffer for cell counting.

Bone marrow cells were isolated by flushing femurs with MACS buffer. Cells were then dispersed with a 5 mL syringe and pass through a 70  $\mu\text{m}$  cell strainer and likewise suspended for counting.

A cell suspension of 100  $\mu\text{L}$  of cells from spleen and bone marrow was stained with a mix of superficial fluorochrome-conjugated antibodies mix prepared in MACS buffer at 4°C for 30 minutes in the dark. Cells were washed twice and resuspended with MACS buffer if analysed immediately, whereas they were fixed/permeabilized (Anti-Mouse/Rat Foxp3 Staining Set APC) for 30 minutes at 4°C for intracellular staining.

In this case, cells were stained with fluorochrome conjugated–Ki67 antibody in 1 $\times$  permeabilization buffer for 30 minutes at 4°C, washed with 1 $\times$  permeabilization buffer and resuspended in MACS buffer.

Antibodies for the following markers were used to identify immune populations: in the blood, CD45 was used for identification of total leukocytes, CD3 for T lymphocytes, CD19 for B lymphocytes, CD11b for cells of myeloid lineage, Ly6G for neutrophils, Ly6C for monocytes (highly expressed on activated while low expressed on resting monocytes). In the bone marrow within the CD11b<sup>+</sup> cells, the combination of the expression of Ly6C versus CD115 allowed to discriminate myeloid precursors as follows: Ly6C<sup>+</sup>CD115<sup>+</sup> for monocyte precursors (MP), Ly6C<sup>+</sup>CD115<sup>-</sup> for granulocyte precursors (GP) and Ly6C<sup>-</sup>CD115<sup>-</sup> for granulocyte and monocyte precursors (GMP). Within MP, the discrimination between cells positive for Ly6G allowed the identification of immature (Ly6G<sup>+</sup>) or mature (Ly6G<sup>-</sup>) monocytes. In the spleen, in addition of markers used in the blood, macrophages were identified as CD11b<sup>+</sup>F4/80<sup>+</sup>, while dendritic cells as CD11c<sup>+</sup>MHCII<sup>+</sup>.

### **2.7 Platelet/leukocyte aggregates.**

Twenty  $\mu\text{L}$  whole blood were stimulated at RT for 5 minutes with 5  $\mu\text{M}$  ADP, then 200  $\mu\text{L}$  of Cell Blood Lysis Buffer (BD Biosciences) were added for 15 minutes, and then samples were stained with saturating concentrations of anti-CD45 (leukocytes), anti-CD41 (platelets), and anti-CD14 (monocytes) or anti-Lys6G (neutrophils) or isotype controls at RT for 30 minutes in the dark. Aggregates were counted by flow FACS “Novocyte3000”. A minimum of 5,000 events were collected in the CD14<sup>+</sup> or Lys6G<sup>+</sup> gate as previously described (Sandrini et al., 2017).

### **2.8. En face analysis of the aorta and aortic sinus histology**

*2.8.1. En face.* Aorta images were captured with a stereomicroscope-dedicated camera (IC80 HD camera, MZ6 microscope, Leica Microsystems, Germany), and analysed with ImageJ image processing program (Schneider et al., 2012). Two independent operators, blinded to the dietary treatments, quantified atherosclerosis extent as percentage of area covered by plaque.

*2.8.2. Aortic sinus histology.* Hearts were removed, fixed in 10% formalin and processed as previously described (Vik et al., 2013). Serial cryosections (7 micron thick) of the aortic sinus were cut and stained with hematoxylin and eosin (H&E) to detect plaque area, calculated as the mean area of those sections showing the three cusps of the aortic valves. The Nanozoomer S60 (Hamamatsu Photonics, Japan) scanner was used to acquire digital images that were subsequently processed with the NDP.view2 software (Hamamatsu Photonics, Japan). Two blinded operators to dietary treatments quantified plaque size.

**2.9. Liver, abdominal WAT, spleen and kidney histology.** Formalin fixed organs/tissues were dehydrated in a graded scale of ethanol, and paraffin embedded (Howard et al., 2018). Sections (4 micron thick) were cut and stained with H&E. Perls' iron staining was used to confirm the presence of hemosiderin in kidney and liver. All histological and histochemical features were assessed by a veterinary pathologist blinded to treatments.

**2.10. Skin histology.** At sacrifice, skin biopsies were excised from the thoracic region, dissected in smaller fragments, and processed for light microscopy analysis. For each animal, skin biopsies were divided in both fragments of 5×5 mm and 2×2 mm.

Fragments of 5×5 mm were immersion-fixed in 4% paraformaldehyde buffered with Phosphate Buffered Saline (PBS) 0.1 M (pH 7.4) for 5 hours at room temperature, dehydrated with ethanol and paraffin embedded. Four µm serial sections were stained with H&E to observe skin morphology at the structural level.

For transmission electron microscopy, skin specimens of 2×2 mm were processed as previously described (Arnaboldi et al., 2015). Semithin sections, 2 µm thick, were stained with toluidine blue.

All sections were observed with a Nikon Eclipse E600 microscope equipped with a Nikon digital camera DXM1200 (Nikon, Tokyo, Japan).



**2.11. RNA extraction and cDNA synthesis.** Total RNA was isolated from mouse tissues and extracted as previously described (Manzini et al., 2018). RNA was quantified and purity was checked, and 1 µg RNA was retrotranscribed to cDNA, as described (Manzini et al., 2015). Possible gDNA contamination was ruled out by running a PCR on 20 ng of cDNA/RNA with a primer pair producing two amplicons of different size on cDNA (193 bp) and gDNA (677 bp). Conditions as follows: 95 °C for 3 min, followed by 35 cycles of 30 s at 95 °C, 30 s at 58.5 °C, 45 s at 72 °C for 45 s, followed by a final amplification step of 5 min at 72 °C, with primers mmu\_Srp14\_f: 5'-GGAGGCTTCTGCTGACGGCG-3' and mmu\_Srp14\_r: 5'-GGGCTCGAGGCCCTCCACA-3'.

**2.12. Quantitative PCR.** Twenty ng of cDNA were used as template for each qPCR reaction, performed on a CFX Connect thermal cycler with iTAQ Universal Sybr Green Supermix. Standard fast cycling conditions were used, with 300 nM primer pairs detailed in Supplementary Table 1. A final melting curve analysis was always performed. Fold changes relative to Control group were calculated with the  $\Delta\Delta C_t$  method (Livak and Schmittgen, 2001). The gene cyclophilin A (Ppia) was used as reference gene.

**2.13. Statistical analyses.** Statistical analyses are detailed for each individual analysis in the appropriate figure or table caption. The threshold for statistical significance was set at  $p = 0.05$ . Analyses were performed with R, version 3.3.3 (R Core Team, 2017), with packages reshape (Wickham, 2007) and PMCMR for Kruskal-Wallis Conover's post hoc (Pohlert, 2014).

## 2.14. Materials

Item	Type	Supplier	City	Country
Scobis uno	Animal bedding	Mucedola	Settimo Milanese	Italy
Adjusted calories 42% from fat, 0.2% cholesterol	Animal diet	Mucedola	Settimo Milanese	Italy
Anti-mouse CD45 FITC-conjugated COD:553079	Antibody	BD bioscience	Franklin Lakes	USA
Anti-mouse CD3 PerCP-Cy5.5-conjugated COD:560527	Antibody	BD bioscience	Franklin Lakes	USA
Anti-mouse CD19 PE-CF594-conjugated COD:562329	Antibody	BD bioscience	Franklin Lakes	USA
Anti-mouse CD11b APC-Cy7-conjugated COD:561039	Antibody	BD bioscience	Franklin Lakes	USA
Anti-mouse CD115 PE-conjugated COD:565249	Antibody	BD bioscience	Franklin Lakes	USA
Anti-mouse Gr-1(Ly6C/Ly6G) BV605-conjugated COD:563299	Antibody	BD bioscience	Franklin Lakes	USA
Anti-mouse F4/80 Af647-conjugated COD:565854	Antibody	BD bioscience	Franklin Lakes	USA
Anti-mouse MHCII BV650-conjugated COD:563415	Antibody	BD bioscience	Franklin Lakes	USA
Anti-mouse CD11c BV786-conjugated COD:563735	Antibody	BD bioscience	Franklin Lakes	USA
Anti-mouse Ki67 V450-conjugated COD:561281	Antibody	BD bioscience	Franklin Lakes	USA
FITC Rat Anti-Mouse CD41 COD: 553848	Antibody	BD bioscience	Franklin Lakes	USA
PE Rat Anti-Mouse CD45	Antibody	BD Pharmingen	San Jose	USA
PE Rat anti-Mouse CD14	Antibody	BD Pharmingen	San Jose	USA
Biotin anti-mouse Ly-6G Antibody	Antibody	eBioscience	San Diego	USA
Anti-mouse CD206 PECy7-conjugated COD:25-2069-41	Antibody	eBioscience	Waltham	USA
Cholesterol assay - COD:CP A11 A01634	Assay/kit	ABX Diagnostics	Montpellier	France
Tryglycerides assay - COD:CP A11 A01640	Assay/kit	ABX Diagnostics	Montpellier	France
High Capacity cDNA Reverse Transcription Kit COD:4368814	Assay/kit	Applied Biosystems	Foster City	USA
Phospholipids assay	Assay/kit	B.L. Chimica	Concorezzo	Italy
iTAQ Universal Sybr Green Supermix	Assay/kit	Bio-Rad	Segrate	Italy
Anti-Mouse/Rat Foxp3 Staining Set APC COD:77-5775-40	Assay/kit	eBioscience	Waltham	USA
Foxp3 / Transcription Factor Staining Buffer Set	Assay/kit	eBioscience	Waltham	USA
Clauss Fibrinogen	Assay/kit	Futura System	Roma	Italy
NucleoSpin RNA extraction kit	Assay/kit	Macherey-Nagel	Duren	Germany
PCR primer	Assay/kit	MWG	Ebersberg	Germany

Vectastain Elite ABC-Peroxidase Staining kit	Assay/kit	Vector Laboratories	Burlingame	USA
Mayer's hematoxylin	Chemical	Bio-Optica	Milano	Italy
Eosin Y alcoholic solution	Chemical	Bio-Optica	Milano	Italy
1-step Fix/Lyse solution COD:00-5333-54	Chemical	eBioscience	Waltham	USA
Red Cell Blood Lysis Buffer COD:00-4300-54	Chemical	eBioscience	Waltham	USA
Durcupan	Chemical	Fluka	Milano	Italy
OCT	Chemical	Sakura Finetek	Alphen aan den Rijn	The Netherlands
Other chemicals	Chemical	Sigma-Aldrich	St. Louis	USA
3,3'-diaminobenzidine substrate (DAB)	Chemical	Vector Laboratories	Burlingame	USA
Isoflurane	Drug	Merial Animal	Woking	UK
Ultra Touch Glucometer	Instrument	LifeScan	Milano	Italy
Miniplast sampling tubes for blood cytology	Plasticware	LP Italiana	Milano	Italy

### 3. Results.

**3.1. Fenretinide treatment reduced weight gain without lowering food intake.** At randomization (day 0), the body weight of the two EKO groups was comparable, as well as that of WT groups: EKO-Ctrl mice weighed  $19.4 \pm 0.9$  g and EKO-Fen  $19.4 \pm 0.7$  g ( $p=0.90$ ); the weight of WT-Ctrl was  $17.2 \pm 0.9$  g and that of WT-Fen was  $17.4 \pm 1.1$  g ( $p=0.94$ ). The growth curves of the four groups during the experimental study are shown in Figure 1A. Fenretinide treatment reduced the weight gain of both EKO and WT mice, with differences that reached statistical significance vs their respective controls starting from day 52 and day 61 of treatment, respectively. At sacrifice, the mean body weight of EKO-Fen was 10.0% lower than that of EKO-Ctrl ( $p=1.3 \times 10^{-5}$ ) and WT-Fen mice weighed 16.5% less than WT-Ctrl ( $p=0.007$ ). This reduction was paralleled by a strong decrease of WAT. Indeed, the abdominal WAT, used as a proxy, showed a strong reduction in both WT-Fen (-58.1%) and EKO-Fen (-74.8%) mice (Supplementary Figure 1).

Food and water intake were periodically monitored (Figure 1B, 1D). Daily food intake, normalized to body weight, was comparable between EKO-Ctrl and EKO-Fen ( $0.121 \pm 0.02$  and  $0.123 \pm 0.02$  g/g body weight, respectively,  $p=0.37$ , Figure 1C). Conversely, food intake of WT-Fen mice was about 12% higher than that of WT-Ctrl mice ( $0.134 \pm 0.01$  vs  $0.119 \pm 0.01$  g/g body weight,  $p=0.008$ , Figure 1C).

From the beginning of the study, an increased water intake was recorded in fenretinide-treated mice (Figure 1D), resulting in an higher normalized daily water intake in both fenretinide-treated groups, being  $0.183 \pm 0.02$  ml/g body weight in EKO-Fen vs  $0.143 \pm 0.01$  in EKO-Ctrl ( $p=0.0002$ ), and  $0.175 \pm 0.04$  in WT-Fen vs  $0.145 \pm 0.01$  in WT-Ctrl ( $p=0.0008$ ) (Figure 1E).

**3.2. Fenretinide treatment lowered plasma glucose levels in EKO mice.** At baseline, after 5 hours fast, lower glucose levels were detected in EKO-Fen mice ( $118.8 \pm 33.4$  mg/dl) compared with EKO-Ctrl mice ( $147.6 \pm 20.7$  mg/dl,  $p=0.006$ ) (Figure 2A). During the glucose challenge, the mean glucose concentrations were lower in treated mice than in controls, but statistical significance was not attained, also when considering the area under the curve (AUC,  $p=0.065$ ) (Figure 2B). At the end of the challenge, i.e. at 100 minutes, and at the regaining of baseline at 125 minutes, glucose levels returned to be significantly lower in EKO-Fen than in EKO-

Ctrl mice ( $129.6 \pm 22.8$  vs  $157.6 \pm 21.5$  mg/dl at 125 minutes,  $p=0.001$ ), consistent with pre-challenge values.

GLUT-4 (*Slc2a4* gene) expression was almost twofold higher in the WAT of EKO-Fen, with respect to EKO-Ctrl ( $p=1.7 \times 10^{-5}$ ) (Figure 3A). Additionally, Resistin (*Retn* gene) expression in WAT was almost fivefold decreased in EKO-Fen with respect to EKO-Ctrl ( $p=0.033$ ) (Figure 3A).

Histological features in WAT were not different among groups. In the liver, a severe decrease in the amount of glycogen stored in the cytoplasm of hepatocytes was observed in EKO-Fen compared to EKO-Ctrl ( $p=5.1 \times 10^{-4}$ ) (Supplementary Figure 2); a mild decrease was also observed in WT-Fen mice compared to WT-Ctrl (Supplementary Table 5).

**3.3. Fenretinide reduced plasma lipid concentrations in EKO.** At the end of treatment, plasma lipid concentrations were measured in EKO mice after 5 hours fasting. Fenretinide treatment strongly lowered plasma lipid levels (Figure 4A). Total cholesterol (TC) levels were reduced by 20.1% ( $1,133.5 \pm 153.3$  mg/dl in EKO-Ctrl vs  $904.5 \pm 169.37$  mg/dl in EKO-Fen,  $p=8.0 \times 10^{-5}$ ) and this decrease was mostly attributable to a cholesterol reduction in the LDL fraction, as assessed by FPLC analysis (Figure 4B). Triglyceride (TG) levels were also dramatically reduced ( $-66.8\%$  vs EKO-Ctrl), averaging at  $114.6 \pm 38.0$  in EKO-Ctrl and  $38.0 \pm 14.9$  mg/dl in EKO-Fen (Figure 4A,  $p=2.1 \times 10^{-11}$ ). This reduction affected all lipoprotein classes (Figure 4C). Last, phospholipids also showed a reduction with fenretinide treatment ( $-20.1\%$ ), averaging at  $350.8 \pm 45.0$  mg/dl in EKO-Ctrl and  $280.09 \pm 143.2$  mg/dl in EKO-Fen ( $p=0.042$ ) (Figure 4A).

Histological examination of liver showed that the high-fat diet in EKO-Ctrl mice caused steatosis, which was severely lowered by Fenretinide treatment ( $p=0.0041$ ) (Supplementary Figure 2). Steatosis was not observed in WT-Ctrl and WT-Fen mice (Supplementary Table 5).

In the liver of treated animals, fenretinide caused a threefold induction of *Hmgcr* ( $p=0.016$ ) and a small, but significant downregulation of SR-B1 (*Scarb1* gene,  $p=6.6 \times 10^{-4}$ ) (Figure 3B). No significant changes in the expression of the other investigated genes relevant to lipid/lipoprotein metabolism were observed (Figure 3B).

### **3.4. Fenretinide dramatically worsened atherosclerosis development in EKO mice.**

Atherosclerotic plaque development was measured on aortas cut lengthwise, as percentage of area occupied by plaques, in the three aortic districts. In each segment, plaque development in fenretinide-treated mice was higher with respect to control mice (Figure 5A). Specifically, plaque development was 32.1%, 190.8% and 129.7% higher in EKO-Fen with respect to EKO-Ctrl at the aortic arch ( $p=0.0003$ ), thoracic ( $p=2.6\times 10^{-9}$ ) and abdominal aorta ( $p=1.3\times 10^{-5}$ ), respectively (Figure 5B).

Plaque extent was further quantified at the aortic sinus (Figure 5C,D) and provided similar results: plaque area was increased by 50.8% in EKO-Fen with respect to EKO-Ctrl ( $p=3.0\times 10^{-7}$ ).

### **3.5. Fenretinide dramatically increased blood leukocytes and affected erythrocyte and platelet counts.**

Total white blood cell counts were significantly increased upon fenretinide treatment, in both EKO (+131.2%) and WT mice (+112.6%) (Figure 6A). Monocytes and eosinophils were unchanged in control and treated mice, but lymphocyte counts were significantly higher, over twofold increased, in both EKO and WT mice (Figure 6B). Also neutrophils were increased upon fenretinide treatment, even if the difference was significant only in WT mice (Figure 6B).

Erythroid parameters decreased in treated animals either in EKO (RBC: -25.0%, HGB -19.8%, HCT -6.7%) or in WT mice (RBC -11.3%, HGB -13.6%, HCT -10.0%). All the differences above were statistically significant, except for the HCT of EKO mice (Figure 6C). In EKO-Fen mice, RBC were macrocytic (MCV +19.0%) and hypochromic (MCHC -14.4%) compared with EKO-Ctrl. In WT mice, RBC were hypochromic (MCHC -3.5%) but no changes in the MCV were observed (Figure 6C). Platelet counts were lower in treated mice compared with controls in both groups, but this decrease was significant only in EKO mice (-19.1%) (Figure 6D).

In bone marrow, an increase of the myeloid:erythroid ratio was found in both groups, but a significant difference was reached only in WT mice (+39.4%). No other significant difference was found, although in both groups lymphocytes and plasma cells showed a moderate reduction in treated mice. The percentage of the proliferating pools of erythroid and myeloid cells was not significantly affected by treatment, but showed an opposite trend in EKO and WT mice (Figure 6E).

### 3.6. Immunophenotyping of blood, bone marrow and spleen

The increase of total counts of circulating leukocytes (CD45+) upon fenretinide treatment was further confirmed by flow cytometry in both EKO and WT mice (+67% and +139%, respectively, Figure 7A, 7D).

In EKO mice this effect was mainly due to the rise of both T (CD3+) and B (CD19+) lymphocytes (Figure 7B). Within monocytes, fenretinide treatment in EKO also increased the relative amount of activated versus resting cells (Ly6C<sup>hi</sup> versus Ly6C<sup>lo</sup>) (Figure 7C). In WT animals, fenretinide treatment caused a significant increase in all leukocyte subpopulations (Figure 7E).

The analysis of bone marrow did not unmask significant differences in the total count of leukocytes (CD45+/femur, Figure 7G) in both EKO and WT mice upon fenretinide treatment. However, the relative amount of myeloid cells (CD11b+) over the total leukocytes revealed an enrichment of this cell type in fenretinide treated animals of both mouse lines (Figure 7H). In addition, in EKO mice fenretinide treatment significantly increased the relative amount of monocyte progenitors (MP) (Figure 7I,J) and showed a significant impairment of monocyte maturation (Figure 7K). No variations by treatment were instead observed in WT mice (Figure 7L,M).

In the spleen, absolute counts of myeloid cells (CD11b), dendritic cells, macrophages, T and B lymphocytes, and consequently of total leukocytes were unaltered in EKO mice (Figure 7N,P). An increase of leukocyte subsets was instead overall observed in the spleen of WT mice, that was significant for myeloid cells (+42.1%), dendritic cells (+74.7%), macrophages (+53.1%), B lymphocytes (+58.2), total leukocytes (+48.9%), (Figure 7O,Q). When cellular count was corrected for spleen weight, the number of all main classes of leukocytes was significantly decreased in EKO mice (Figure 7R,T: -54.9%, -48.3%, -52.9%, -60.8%, -60.9%, -59.8% for myeloid, dendritic cells, macrophages, T and B lymphocytes, total leukocytes, respectively) whereas no differences were detected in WT mice (Figure 7S,U). These findings are in accordance with the morphological changes observed in both genotypes following fenretinide treatment. In WT mice, spleen weight was moderately increased (90±20 mg and 120±40 mg in WT-Ctrl and WT-Fen, respectively; p=0.035), whereas in EKO mice the spleen appeared markedly enlarged (211±67 mg and 597±159 mg in EKO-Ctrl and EKO-Fen, respectively; p=7.8×10<sup>-12</sup>) (Supplementary Figure 1). In WT-Fen, histological examination showed an increased, although not significant, incidence of extramedullary hematopoiesis, characterized by the presence of hematopoietic cells

expanding the red pulp (Supplementary Table 5). On the contrary, in EKO-Fen mice, compared to EKO-Ctrl mice, spleen parenchyma showed the presence of severe extramedullary hematopoiesis ( $p=0.008$ ) and a marked follicular atrophy ( $p=0.006$ ) (Supplementary Table 2 and Figure 8A,B). Extramedullary hematopoiesis was also a constant finding in the liver of EKO-Fen (9 out of 10 animals), but not in that of EKO-Ctrl (1 out of 10 mice,  $p=0.0011$ ) (Figure 8C,D).

### **3.7. Fenretinide increased erythrocyte destruction.**

Histological findings in kidney and liver indicated that fenretinide treatment to EKO mice accelerated erythrocyte turnover. In fact, hemosiderosis was absent in the kidney and liver of EKO-Ctrl and WT mice (Supplementary Table 5), whereas in EKO-Fen the presence of hemosiderin was observed multifocally within the cytoplasm of tubular epithelial cells in the proximal convoluted tubules of the kidney in all animals (Figure 8G-L and Supplementary Table 3) and in the cytoplasm of Kupffer cells in the liver of 9 out of 10 mice (Figure 8E,F).

### **3.8. Functional fibrinogen**

A significant increase in the plasma fibrinogen activity was observed in EKO-Fen mice, with respect to EKO-Ctrl (+48.7%,  $p=0.0371$ ) (Supplementary Figure 3). The same trend was observed in WT mice (+31.0%), although it did not reach statistical significance.

### **3.9. Platelet/leukocyte aggregates.**

In total blood, the percentage of platelet-leukocyte aggregates was greater in EKO-Ctrl compared with WT-Ctrl mice ( $p=0.0338$ ) (Supplementary Figure 4A). This parameter was not modified by fenretinide treatment in WT mice, whereas it was strongly lowered in EKO animals, where it became comparable to that of WT mice (Supplementary Figure 4A).

Remarkably, the analysis of leukocyte subsets showed that the percentage of monocyte & neutrophil-platelet aggregates was much higher in EKO-Ctrl vs WT-Ctrl mice (+112.81%,  $p=0.00107$ ) and fenretinide treatment only slightly modified these values, in both genotypes ( $p>0.05$ , Figure 9A).

When considering monocyte-platelet aggregates alone, untreated mice of both genotypes showed similar values (Figure 9B). Fenretinide tended to decrease the



number of monocyte-platelet aggregates in WT mice (from  $25.4 \pm 7.2\%$  to  $15.1 \pm 3.8\%$ ,  $p=0.058$ ), whereas in EKO mice, the treatment significantly increased the number of aggregates (+42.3%, from  $27.8 \pm 6.7\%$  to  $42.3 \pm 6.8\%$ ,  $p=0.0081$ ) (Figure 9B).

Finally, the percentage of circulating neutrophil-platelet aggregates was greater in EKO-Ctrl compared to WT-Ctrl mice ( $p=0.0159$ ). Fenretinide treatment did not cause any significant variation in the two genotypes (Supplementary Figure 4B).

### 3.10 Other histological findings.

In lungs, moderate to severe lesions characterized by the presence of foamy macrophages were a constant finding in EKO-Fen mice (Supplementary Figure 5), whereas they were absent in EKO-Ctrl as well as in all WT animals (Supplementary Table 5). Additionally, cholesterol crystals were occasionally observed only in EKO-Fen animals.

Morphological analysis did not show any significant difference between the skin of treated and untreated WT mice (Supplementary Table 4). In both the experimental groups, indeed, the epidermis appeared build-up of ordinated overlapped layers of cells and in the dermis there were no signs of alteration. The presence of foam cells was detected only in treated and untreated EKO mice ( $p= 0.000113$  vs WT mice). Other morphological alterations were also visible, although shared almost equally in EKO-Ctrl and EKO-Fen animals (Supplementary Table 4 and Supplementary Figure 6)

#### 4. Discussion

The main result of the present study is that, despite the favourable metabolic effects exerted by fenretinide treatment on glucose tolerance, fat mass accumulation, liver steatosis and, most importantly, on the plasma lipid levels, the treatment resulted into an unpredictable worsening of atherosclerosis. In the study, apoE-deficient mice were used, as they spontaneously develop hypercholesterolemia and atherosclerotic lesions that, alike human counterparts, stem from early fatty streaks and develop into advanced and complex lesions (Plump et al., 1992; Nakashima et al., 1994). When fed high-fat diet, lesion formation is greatly accelerated. Further, this dietary treatment also results in an impaired glucose metabolism (Nakashima et al., 1994; Su et al., 2006). Wild-type mice on the same background were also included in the study to assess genotype-specific biases.

Fenretinide pharmacodynamics and toxicology have been known for a long time, and a dietary formulation is possible (McCormick et al., 1987; Slawin et al., 1993; Preitner et al., 2009). A formulation of 1 mg fenretinide per g of diet has been chosen as proof-of-principle. A long-term treatment (12 weeks) has already been documented in diet-induced obese mice fed with high fat diet supplemented with the selected fenretinide dosage (0.1% w/w) and even longer treatment times have been used (Preitner et al., 2009). As readout of the treatment, the hepatic expression of Cyp26a1, a cytochrome involved in the metabolism of retinoids, was upregulated fourfold in the liver of fenretinide-treated mice (Figure 3B).

The possible effects of fenretinide treatment on body weight, fat mass accumulation, glucose metabolism and plasma lipid levels, still untested in the apoE-deficient model, were investigated in the present study. The reduction of body weight gain following fenretinide treatment has been thoroughly documented in wild-type and in genetically obese mice (Preitner et al., 2009; Koh et al., 2012; Mcilroy et al., 2013; Shearer et al., 2015). Consistent with these findings, in the present study fenretinide treatment reduced body weight gain and fat mass in both apoEKO and wild-type mice. This mostly occurs via the inhibition of adipogenesis through prevention of C/EBP $\beta$  transcription (Mcilroy et al., 2016). The treatment was not expected to alter the food intake (Shearer et al., 2015), and indeed food intake was unchanged in EKO and negligibly increased in WT mice.

It has also been demonstrated how fenretinide displays insulin-sensitizing and anti-diabetic effects in mice and overweight humans (Bikman et al., 2012). Reportedly, the inhibition of ceramide pathway biosynthesis enhances insulin sensitivity (Aerts et al., 2007), and fenretinide has been found to be inhibiting dihydroceramide desaturases, that catalyse the final step in *de novo* ceramide synthesis (Rahmaniyan et al., 2011). Likewise, in the present study fenretinide treatment resulted in significantly lower basal glycaemia in treated vs untreated EKO mice. Furthermore, throughout the whole glucose tolerance test, treated EKO mice always showed average glucose levels trending towards 10-20% lower values than untreated mice. Slc2a4 (GLUT4) expression levels correlate with whole-body insulin-mediated glucose homeostasis (Atkinson et al., 2013). Moreover, insulin-resistant glucose transport in adipocytes from obese and diabetic subjects correlates with reduced GLUT4 expression (Berger et al., 1989). Accordingly, we found that Slc2a4 expression was almost twofold higher in the WAT of EKO-Fen, with respect to controls.

In mice, the main source of resistin (Retn gene) is white adipose tissue (Jamaluddin et al., 2012). Even if resistin was first described as a factor contributing to the development of insulin resistance and diabetes in humans, there is no clear consensus yet regarding its exact contribution to obesity and insulin sensitivity. However, resistin serum levels are positively associated with increased acute coronary syndrome (Jamaluddin et al., 2012). Further, several studies support a positive correlation between elevated serum resistin and obesity or impaired glucose tolerance (Malo et al., 2011; Luo et al., 2012). We found that Retn gene expression in WAT was almost fivefold decreased in EKO-Fen with respect to EKO-Ctrl.

Another reported beneficial effect of fenretinide treatment is the reduction of plasma lipids, including total cholesterol, triglycerides and free fatty acids, in obese mice fed a high fat diet (Koh et al., 2012). This holds true also in EKO mice, where fenretinide was able to dramatically and significantly reduce total cholesterol (-20.2%), triglycerides (-66.9%) and phospholipids (-20.1%). No relevant variations in the expression of genes involved in lipid metabolism were found, except for a threefold increase of Hmgcr, the rate-limiting enzyme in cholesterol synthesis. Additionally, hepatic steatosis and glycogen accumulation, typically observed in EKO mice on high fat diet, were greatly reduced by treatment.

Given the wealth of favourable preliminary data, the main objective of the present study was the evaluation of a possible effect of fenretinide on atherosclerosis

development. Strikingly, and in apparent contrast with the data discussed above, the treatment resulted in a marked increase of the extent of atherosclerotic lesions in all aortic districts, including the aortic sinus. This result may not be explained taken into account the data reviewed so far, especially considering the reduction of plasma lipid levels. While it is true that there was a remarkable absolute reduction of total cholesterol (-229 mg/dl), plasma cholesterol levels remained very high, a characteristic feature of this mouse model. Nonetheless, this reduction in the lipid levels, however limited, should be paralleled by a reduced plaque development (Parolini et al., 2017).

The most remarkable macroscopic feature of EKO mice treated with fenretinide was an abnormally enlarged spleen. Also in WT mice the treatment resulted in significantly heavier spleens, although this variation was less dramatic. Whereas in WT mice this weight increase was paralleled by an increase in the leukocyte content, in EKO mice the augmented organ mass was not associated to a change of total leukocyte number, as well as of individual leukocyte subpopulations, that were totally comparable in treated and untreated EKO mice. The histological analysis supported these findings, being the spleen of treated EKO mice characterized by small and atrophic follicles. Extramedullary haematopoiesis was detected in fenretinide treated WT mice as well as EKO mice. In these latter, the red pulp was strongly expanded, thus explaining, at least in part, the enlargement of this organ. Only in EKO treated mice, extramedullary haematopoiesis was observed also in the liver.

Blood cytology analysis showed that in both EKO and WT mice, the treatment induced a decrease of the erythroid mass. This decrease seemed to be due to a reduced production of RBC in WT mice, which had a normocytic hypochromic pattern. Conversely, in EKO mice the macrocytic hypochromic pattern was consistent with active bone marrow regeneration, generally associated to blood loss or hemolysis. Histopathological findings strongly supported this latter hypothesis, showing in the kidney, as well as in hepatic Kupffer cells, a massive deposition of hemosiderin pigment, coming from disintegrating erythrocytes. Erythrolysis was a condition found only in EKO mice and possibly consequent to the severe hypercholesterolemia that has been shown to increase the osmotic fragility of RBC (Fessler et al., 2013). In addition, fenretinide treatment is associated to an augmented ROS production (Cuperus et al., 2010) which in turn reduces RBC deformability (Diederich et al., 2018). These two effects synergize in EKO-Fen only, leading to peripheral hemolysis.

Fenretinide treatment caused a dramatic increase of circulating leukocytes both in WT and EKO mice. All leukocyte classes contributed to this rise, with lymphocytes playing the major role. A similar response to fenretinide treatment has been recently reported in wild-type mice receiving higher doses of the drug (Cook et al., 2018). Being fenretinide tested in the clinic for the treatment of solid and blood malignancies, it is difficult to translate this finding in humans.

Platelet counts were lower in EKO compared to WT mice. In EKO however, large platelet clumps were frequently found in blood, suggesting that this decrease is likely due to an hyperactivation of platelets. Fenretinide treatment lowered platelet counts in both genotypes, although this trend was particularly severe, and statistically significant, only in EKO mice.

The hematological alterations discussed above, consequent to fenretinide treatment could at least partially explain the atherosclerosis worsening observed in EKO mice.

The peripheral destruction of erythrocytes observed in EKO treated mice has been reported to release inflammatory mediators, resulting in a state of general inflammation (Randolph, 2009). Additionally, the percentage of circulating activated monocytes was increased by treatment. Monocytes are the primary inflammatory cell type that infiltrates early atherosclerotic plaques, and their recruitment drives disease progression (Randolph, 2009). Interestingly, FACS analyses revealed an increase in the bone marrow of myeloid precursors, including immature monocytes, in EKO treated mice, suggesting an accelerated myelopoiesis and an impaired maturation of these lineages. Of note, increased bone marrow myelopoiesis and extramedullary myelopoiesis have been positively associated with atherosclerosis (Yvan-Charvet et al., 2010; Murphy et al., 2011); in addition, our observation that circulating activated monocytes are increased in treated EKO further links the immunomodulation induced by fenretinide to atherosclerosis development. Further, the greater percentage of monocyte/platelet aggregates detected in treated EKO mice might contribute to the marked atherosclerosis in these mice. Indeed, activated platelets bound circulating monocytes, promoting atherosclerotic plaque formation and development (Huo et al., 2003). In particular, both activated platelets and platelet-monocyte aggregates induce the adhesion of leukocytes to the endothelium, the recruitment of monocytes in atherosclerotic lesion, and they increase cholesteryl ester accumulation in monocyte-derived macrophages, as well as the differentiation of CD34<sup>+</sup> myeloid cells into foam cells (Daub et al., 2006).

Finally, the increased fibrinogen activity in EKO mice treated with fenretidine and the greater concomitant increase in atherosclerosis is coherent with data obtained in various epidemiological studies and animal models (Handa et al., 1989; Koopman et al., 1997; Uner et al., 2018).

In conclusion, all these evidences demonstrate that fenretinide treatment, in spite of positive metabolic effects, severely altered blood cell turnover, resulting in a worsening of atherosclerosis development in an atherosclerosis-prone mouse model of widespread use (Emini Veseli et al., 2017). Even if more work is needed to demonstrate to what extent they can be translated into the human setting, these results strongly suggest careful selection and monitoring of patients undergoing fenretinide treatment.

For Peer Review

## 5. Author Contributions

Marco Busnelli: Conceived the study, managed the study, evaluated atherosclerosis development, wrote the paper

Stefano Manzini: Conceived the study, managed the study, performed molecular biology experiments, performed statistical analyses, wrote the paper

Fabrizia Bonacina: Performed FACS experiments

Sabina Soldati: Performed extensive histological analyses

Silvia Stella Barbieri: Assayed leukocyte-platelet interactions, assayed functional fibrinogen

Patrizia Amadio: Assayed leukocyte-platelet interactions, assayed functional fibrinogen

Leonardo Sandrini: Assayed leukocyte-platelet interactions, assayed functional fibrinogen

Francesca Arnaboldi: Performed skin histology

Elena Donetti: Performed skin histology

Reijo Laaksonen: Helped conceiving the study, proofread the manuscript

Saverio Paltrinieri: Performed extensive hematological analyses and bone marrow cytology

Eugenio Scanziani: Performed extensive histological analyses

Giulia Chiesa: Conceived the study, managed the study, raised funds for the study, supervised all experiments, critically revised the manuscript

## 6. Acknowledgements

This work was funded by the European Community's Seventh Framework Programme (FP7/2012–2017) RiskyCAD, grant no. 305739 (G.C.), by Fondazione CARIPLO (2011-0645) (G.C.) and by grants from MIUR Progetto Eccellenza. We are grateful to Ms. Elda Desiderio Pinto for administrative assistance. We deeply thank Elena Olmastroni for advices and checks on statistical analyses and we thank Dr. Cinzia Parolini for technical support. Part of this work was carried out at NOLIMITS, an advanced imaging facility established by the Università degli Studi di Milano. Dr. Leonardo Sandrini is supported by the 32<sup>nd</sup> cycle Ph.D. program in “Scienze farmacologiche sperimentali e cliniche”, Università degli Studi di Milano.



## 7. References

- Aburasayn, H., Batran, R. Al, and Ussher, J.R. (2016). Targeting ceramide metabolism in obesity. *Am. J. Physiol. Endocrinol. Metab.* 311: E423-35.
- Aerts, J.M., Ottenhoff, R., Powlson, A.S., Grefhorst, A., Eijk, M. van, Dubbelhuis, P.F., et al. (2007). Pharmacological inhibition of glucosylceramide synthase enhances insulin sensitivity. *Diabetes* 56: 1341–9.
- Amadio, P., Colombo, G.I., Tarantino, E., Gianellini, S., Ieraci, A., Brioschi, M., et al. (2017a). BDNFVal66met polymorphism: a potential bridge between depression and thrombosis. *Eur. Heart J.* 38: 1426–1435.
- Amadio, P., Tarantino, E., Sandrini, L., Tremoli, E., and Barbieri, S.S. (2017b). Prostaglandin-endoperoxide synthase-2 deletion affects the natural trafficking of Annexin A2 in monocytes and favours venous thrombosis in mice. *Thromb. Haemost.* 117: 1486–1497.
- Arnaboldi, F., Busnelli, M., Cornaghi, L., Manzini, S., Parolini, C., Dellerà, F., et al. (2015). High-density lipoprotein deficiency in genetically modified mice deeply affects skin morphology: A structural and ultrastructural study. *Exp. Cell Res.* 338: 105–12.
- Atkinson, B.J., Griesel, B.A., King, C.D., Josey, M.A., and Olson, A.L. (2013). Moderate glut4 overexpression improves insulin sensitivity and fasting triglyceridemia in high-fat diet-fed transgenic mice. *Diabetes* 62: 2249–2258.
- Berger, J., Biswas, C., Vicario, P.P., Strout, H.V., Saperstein, R., and Pilch, P.F. (1989). Decreased expression of the insulin-responsive glucose transporter in diabetes and fasting. *Nature* 340: 70–2.
- Berry, D.C., DeSantis, D., Soltanian, H., Croniger, C.M., and Noy, N. (2012). Retinoic acid upregulates preadipocyte genes to block adipogenesis and suppress diet-induced obesity. *Diabetes* 61: 1112–21.
- Berry, D.C., and Noy, N. (2009). All-trans-retinoic acid represses obesity and insulin resistance by activating both peroxisome proliferation-activated receptor beta/delta and retinoic acid receptor. *Mol. Cell. Biol.* 29: 3286–96.
- Bikman, B.T., Guan, Y., Shui, G., Siddique, M.M., Holland, W.L., Kim, J.Y., et al. (2012). Fenretinide prevents lipid-induced insulin resistance by blocking ceramide biosynthesis. *J. Biol. Chem.* 287: 17426–37.
- Busnelli, M., Manzini, S., Hilvo, M., Parolini, C., Ganzetti, G.S., Dellerà, F., et al.

- (2017). Liver-specific deletion of the Plpp3 gene alters plasma lipid composition and worsens atherosclerosis in apoE<sup>-/-</sup> mice. *Sci. Rep.* 7: 44503.
- Cook, J.C., Obert, L.A., Koza-Taylor, P., Coskran, T.M., Opsahl, A.C., Ziemek, D., et al. (2018). From the Cover: Fenretinide, Troglitazone, and Elmiron Add to Weight of Evidence Support for Hemangiosarcoma Mode-of-Action From Studies in Mice. *Toxicol. Sci.* 161: 58–75.
- Cooper, J.P., Reynolds, C.P., Cho, H., and Kang, M.H. (2017). Clinical development of fenretinide as an antineoplastic drug: Pharmacology perspectives. *Exp. Biol. Med.* (Maywood). 242: 1178–1184.
- Cuperus, R., Leen, R., Tytgat, G.A.M., Caron, H.N., and Kuilenburg, A.B.P. van (2010). Fenretinide induces mitochondrial ROS and inhibits the mitochondrial respiratory chain in neuroblastoma. *Cell. Mol. Life Sci.* 67: 807–16.
- Daub, K., Langer, H., Seizer, P., Stellos, K., May, A.E., Goyal, P., et al. (2006). Platelets induce differentiation of human CD34<sup>+</sup> progenitor cells into foam cells and endothelial cells. *FASEB J.* 20: 2559–61.
- Diederich, L., Suvorava, T., Sansone, R., Keller, T.C.S., Barbarino, F., Sutton, T.R., et al. (2018). On the Effects of Reactive Oxygen Species and Nitric Oxide on Red Blood Cell Deformability. *Front. Physiol.* 9: 332.
- Emini Veseli, B., Perrotta, P., Meyer, G.R.A. De, Roth, L., Donckt, C. Van der, Martinet, W., et al. (2017). Animal models of atherosclerosis. *Eur. J. Pharmacol.* 816: 3–13.
- Fessler, M.B., Rose, K., Zhang, Y., Jaramillo, R., and Zeldin, D.C. (2013). Relationship between serum cholesterol and indices of erythrocytes and platelets in the US population. *J. Lipid Res.* 54: 3177–88.
- Handa, K., Kono, S., Saku, K., Sasaki, J., Kawano, T., Sasaki, Y., et al. (1989). Plasma fibrinogen levels as an independent indicator of severity of coronary atherosclerosis. *Atherosclerosis* 77: 209–13.
- Howard, S.R., Oleari, R., Poliandri, A., Chantzara, V., Fantin, A., Ruiz-Babot, G., et al. (2018). HS6ST1 Insufficiency Causes Self-Limited Delayed Puberty in Contrast With Other GnRH Deficiency Genes. *J. Clin. Endocrinol. Metab.* 103: 3420–3429.
- Huo, Y., Schober, A., Forlow, S.B., Smith, D.F., Hyman, M.C., Jung, S., et al. (2003). Circulating activated platelets exacerbate atherosclerosis in mice deficient in apolipoprotein E. *Nat. Med.* 9: 61–7.
- Jamaluddin, M.S., Weakley, S.M., Yao, Q., and Chen, C. (2012). Resistin: functional

roles and therapeutic considerations for cardiovascular disease. *Br. J. Pharmacol.* *165*: 622–32.

Koh, I., Jun, H.-S., Choi, J.S., Lim, J.H., Kim, W.H., Yoon, J.B., et al. (2012).

Fenretinide ameliorates insulin resistance and fatty liver in obese mice. *Biol. Pharm. Bull.* *35*: 369–75.

Koopman, J., Maas, A., Rezaee, F., Havekes, L., Verheijen, J., Gijbels, M., et al.

(1997). Fibrinogen and atherosclerosis: a study in transgenic mice. *Fibrinolysis and Proteolysis* *11*: 19–21.

Lachance, C., Wojewodka, G., Skinner, T.A.A.A., Guilbault, C., Sanctis, J.B. De, and Radzioch, D. (2013). Fenretinide corrects the imbalance between omega-6 to omega-3 polyunsaturated fatty acids and inhibits macrophage inflammatory mediators via the ERK pathway. *PLoS One* *8*: e74875.

Livak, K.J., and Schmittgen, T.D. (2001). Analysis of relative gene expression data using real-time quantitative PCR and the 2(-Delta Delta C(T)) Method. *Methods* *25*: 402–8.

Luo, R., Li, X., Jiang, R., Gao, X., Lü, Z., and Hua, W. (2012). Serum concentrations of resistin and adiponectin and their relationship to insulin resistance in subjects with impaired glucose tolerance. *J. Int. Med. Res.* *40*: 621–30.

Mackie, I.J., Kitchen, S., Machin, S.J., Lowe, G.D.O., and Haemostasis and Thrombosis Task Force of the British Committee for Standards in Haematology (2003). Guidelines on fibrinogen assays. *Br. J. Haematol.* *121*: 396–404.

Malo, E., Ukkola, O., Jokela, M., Moilanen, L., Kähönen, M., Nieminen, M.S., et al. (2011). Resistin is an indicator of the metabolic syndrome according to five different definitions in the Finnish Health 2000 survey. *Metab. Syndr. Relat. Disord.* *9*: 203–10.

Manzini, S., Busnelli, M., Parolini, C., Minoli, L., Ossoli, A., Brambilla, E., et al. (2018). Topiramate protects apoE-deficient mice from kidney damage without affecting plasma lipids. *Pharmacol. Res.* *141*: 189–200.

Manzini, S., Pinna, C., Busnelli, M., Cinquanta, P., Rigamonti, E., Ganzetti, G.S., et al. (2015). Beta2-adrenergic activity modulates vascular tone regulation in lecithin:cholesterol acyltransferase knockout mice. *Vascul. Pharmacol.* *74*: 114–121.

Marchesi, M., Parolini, C., Caligari, S., Gilio, D., Manzini, S., Busnelli, M., et al. (2011). Rosuvastatin does not affect human apolipoprotein A-I expression in genetically modified mice: a clue to the disputed effect of statins on HDL. *Br. J.*

Pharmacol. *164*: 1460–8.

McCormick, D.L., Bagg, B.J., and Hultin, T.A. (1987). Comparative activity of dietary or topical exposure to three retinoids in the promotion of skin tumor induction in mice. *Cancer Res.* *47*: 5989–93.

Mcilroy, G.D., Delibegovic, M., Owen, C., Stoney, P.N., Shearer, K.D., McCaffery, P.J., et al. (2013). Fenretinide treatment prevents diet-induced obesity in association with major alterations in retinoid homeostatic gene expression in adipose, liver, and hypothalamus. *Diabetes* *62*: 825–36.

Mcilroy, G.D., Tammireddy, S.R., Maskrey, B.H., Grant, L., Doherty, M.K., Watson, D.G., et al. (2016). Fenretinide mediated retinoic acid receptor signalling and inhibition of ceramide biosynthesis regulates adipogenesis, lipid accumulation, mitochondrial function and nutrient stress signalling in adipocytes and adipose tissue. *Biochem. Pharmacol.* *100*: 86–97.

Mody, N., and Mcilroy, G.D. (2014). The mechanisms of Fenretinide-mediated anti-cancer activity and prevention of obesity and type-2 diabetes. *Biochem. Pharmacol.* *91*: 277–86.

Murphy, A.J., Akhtari, M., Tolani, S., Pagler, T., Bijl, N., Kuo, C.-L., et al. (2011). ApoE regulates hematopoietic stem cell proliferation, monocytosis, and monocyte accumulation in atherosclerotic lesions in mice. *J. Clin. Invest.* *121*: 4138–49.

Nakashima, Y., Plump, A.S., Raines, E.W., Breslow, J.L., and Ross, R. (1994). ApoE-deficient mice develop lesions of all phases of atherosclerosis throughout the arterial tree. *Arterioscler. Thromb. a J. Vasc. Biol.* *14*: 133–40.

Parolini, C., Bjørndal, B., Busnelli, M., Manzini, S., Ganzetti, G.S., Delleria, F., et al. (2017). Effect of Dietary Components from Antarctic Krill on Atherosclerosis in apoE-Deficient Mice. *Mol. Nutr. Food Res.* *61*: 1700098.

Parolini, C., Vik, R., Busnelli, M., Bjørndal, B., Holm, S., Brattelid, T., et al. (2014). A salmon protein hydrolysate exerts lipid-independent anti-atherosclerotic activity in ApoE-deficient mice. *PLoS One* *9*: e97598.

Petersen, M.C., and Shulman, G.I. (2018). Mechanisms of Insulin Action and Insulin Resistance. *Physiol. Rev.* *98*: 2133–2223.

Plump, A.S., Smith, J.D., Hayek, T., Aalto-Setälä, K., Walsh, A., Verstuyft, J.G., et al. (1992). Severe hypercholesterolemia and atherosclerosis in apolipoprotein E-deficient mice created by homologous recombination in ES cells. *Cell* *71*: 343–53.

Pohlert, T. (2014). The Pairwise Multiple Comparison of Mean Ranks Package

(PMCMR).

Preitner, F., Mody, N., Graham, T.E., Peroni, O.D., and Kahn, B.B. (2009). Long-term Fenretinide treatment prevents high-fat diet-induced obesity, insulin resistance, and hepatic steatosis. *Am. J. Physiol. Endocrinol. Metab.* 297: E1420-9.

R Core Team (2017). R: A Language and Environment for Statistical Computing.

Rahmaniyan, M., Curley, R.W., Obeid, L.M., Hannun, Y.A., and Kraveka, J.M. (2011). Identification of dihydroceramide desaturase as a direct in vitro target for fenretinide. *J. Biol. Chem.* 286: 24754–64.

Randolph, G.J. (2009). The fate of monocytes in atherosclerosis. *J. Thromb. Haemost.* 7 *Suppl 1*: 28–30.

Sandrini, L., Ieraci, A., Amadio, P., Popoli, M., Tremoli, E., and Barbieri, S.S. (2017). Apocynin Prevents Abnormal Megakaryopoiesis and Platelet Activation Induced by Chronic Stress. *Oxid. Med. Cell. Longev.* 2017:.

Schneider, C.A., Rasband, W.S., and Eliceiri, K.W. (2012). NIH Image to ImageJ: 25 years of image analysis. *Nat. Methods* 9: 671–5.

Shearer, K.D., Morrice, N., Henderson, C., Reekie, J., Mcilroy, G.D., McCaffery, P.J., et al. (2015). Fenretinide prevents obesity in aged female mice in association with increased retinoid and estrogen signaling. *Obesity (Silver Spring)*. 23: 1655–62.

Slawin, K., Kadmon, D., Park, S.H., Scardino, P.T., Anzano, M., Sporn, M.B., et al. (1993). Dietary fenretinide, a synthetic retinoid, decreases the tumor incidence and the tumor mass of ras+myc-induced carcinomas in the mouse prostate reconstitution model system. *Cancer Res.* 53: 4461–5.

Su, Z., Li, Y., James, J.C., Matsumoto, A.H., Helm, G.A., Lusic, A.J., et al. (2006). Genetic linkage of hyperglycemia, body weight and serum amyloid-P in an intercross between C57BL/6 and C3H apolipoprotein E-deficient mice. *Hum. Mol. Genet.* 15: 1650–8.

Uner, A.G., Unsal, C., Unsal, H., Erdogan, M.A., Koc, E., Ekici, M., et al. (2018). Mice with diet-induced obesity demonstrate a relative prothrombotic factor profile and a thicker aorta with reduced ex-vivo function. *Blood Coagul. Fibrinolysis* 29: 257–266.

Vik, R., Busnelli, M., Parolini, C., Bjørndal, B., Holm, S., Bohov, P., et al. (2013). An immunomodulating fatty acid analogue targeting mitochondria exerts anti-atherosclerotic effect beyond plasma cholesterol-lowering activity in apoe(-/-) mice. *PLoS One* 8: e81963.

- Wickham, H. (2007). Reshaping data with the reshape package. *J. Stat. Softw.* *21*:.
- Yvan-Charvet, L., Pagler, T., Gautier, E.L., Avagyan, S., Siry, R.L., Han, S., et al. (2010). ATP-binding cassette transporters and HDL suppress hematopoietic stem cell proliferation. *Science* *328*: 1689–93.
- Zizola, C.F., Frey, S.K., Jitngarmkusol, S., Kadereit, B., Yan, N., and Vogel, S. (2010). Cellular retinol-binding protein type I (CRBP-I) regulates adipogenesis. *Mol. Cell. Biol.* *30*: 3412–20.

For Peer Review

## 8. Figure and figure legends

**Figure 1** – The weight of mice ( $n = 20$  for EKO;  $n = 10$  for BL/6) was monitored 2-3 times a week for a period of 12 weeks total. **(A)** Average weight is plotted and shown within  $\pm 1$  SD for either EKO (left) and BL/6 (right). Weight differences started to become steadily statistically significant starting from day 52 for EKO and day 61 for BL/6. Likewise, food and water intake were monitored per cage (mice were housed 3-4 per cage) and normalized to the number of animals in each cage. Average values and SD are charted for each time point **(B, D)**. For each time point, average intakes were normalized to the average weight of mice in each cage; the average of all measurements is charted for food **(C, †:  $p = 0.0021$ , F-value 12.88)** and water **(E, ‡:  $p = 1.56 \times 10^{-10}$ , F-value 76.46; §:  $p = 6.8 \times 10^{-6}$ , F-value 39.00)**. Unpaired two-tailed Student's T-test was used to test mean differences at each time point **(A)**, significant differences are indicated by \*. Repeated measures ANOVA was used to test for differences between groups throughout the entire duration of the study **(B, D, graphically summarized in C, E respectively)**. Data are shown  $\pm$  SD.

**Figure 2** – After an i.p. injection of 2 g / Kg glucose ( $n = 16$  randomly chosen EKO mice per group), glycaemia has been monitored at intervals of 25 minutes, up to 125 minutes total. Glucose concentration as function of time is charted. \*:  $p = 6.2 \times 10^{-3}$ ; †:  $p = 3.6 \times 10^{-2}$ , ‡:  $p = 1.3 \times 10^{-3}$  **(A)**. Measurements of areas under the curve (AUC) are shown in **B**, in arbitrary units. Repeated measures ANOVA was used to test for statistically significant differences **(A,  $p = 0.0651$ , F-score 3.66)** and by unpaired two-tailed Student's T-test **(B)**. Data are shown  $\pm$  SD.

**Figure 3** – Box plots of gene expression in the abdominal white adipose tissue **(A)** and liver **(B)** are shown ( $n = 12$  randomly chosen EKO mice per group; each sample was run in triplicate). **A:** Fold changes of genes quantified in the abdominal white adipose tissue, relative to EKO-Ctrl group, are charted. \*:  $p = 1.7 \times 10^{-5}$ ; †:  $p = 3.4 \times 10^{-2}$ ; ‡:  $p = 3.2 \times 10^{-4}$ . **B:** Fold changes of hepatic genes, relative to EKO-Ctrl group, are charted. \*:  $p = 6.6 \times 10^{-4}$ ; †:  $p = 1.6 \times 10^{-2}$ ; ‡:  $p = 2.4 \times 10^{-7}$ . Statistically significant differences were determined by unpaired two-tailed Student's T-test. The upper and lower ends of the boxes indicate the 25<sup>th</sup> and 75<sup>th</sup> percentiles, respectively. The length

of the box shows the interquartile range within which 50% of the values are located. The solid gray lines denote the median.

**Figure 4** – Total cholesterol (TC), triglyceride (TG) and phospholipid (PL) levels (n = 20, each sample was assayed in duplicate), quantified after 5 hours fasting, are shown. \*:  $p = 8.0 \times 10^{-5}$ ; †:  $p = 2.1 \times 10^{-11}$ , ‡:  $p = 4.2 \times 10^{-2}$  (A). TC and TG distribution among plasma lipoproteins by FPLC is shown in B and C, respectively. Each profile was obtained from pooled plasma of all mice within each experimental group (n = 20). Statistically significant differences were determined by unpaired two-tailed Student's T-test. Data are shown  $\pm$  SD.

**Figure 5** – Representative image of aortas prepared with the en-face method (A). The aorta (n = 20 per group) was cut lengthwise and pinned flat onto a black wax surface, then the exposed plaques were quantified as a percentage of the whole aortic area; \*:  $p = 3.0 \times 10^{-7}$ ; †:  $p = 3.6 \times 10^{-4}$ ; ‡:  $p = 2.6 \times 10^{-9}$ , §:  $p = 1.3 \times 10^{-5}$  (B). Representative H&E photomicrographs of aortic sinuses (n = 20 per group, C). Plaque extent is reported as square micrometers  $p = 3.1 \times 10^{-7}$  (D). Statistically significant differences were determined by unpaired two-tailed Student's T-test. Data are expressed as mean  $\pm$  SD. Bar length= 500  $\mu$ m.

**Figure 6** – Cytologic evaluation of blood and bone marrow (n = 10 randomly chosen mice per group). RBC: red blood cells (erythrocyte number); WBC: white blood cells; HGB: haemoglobin; HCT: hematocrit; MCV: mean corpuscular volume; MCHC: mean corpuscular haemoglobin concentration; MCH: mean corpuscular haemoglobin; M/E ratio: monocyte to erythrocyte ratio. Statistically significant differences were determined by unpaired two-tailed Student's T-test. Data are expressed as mean  $\pm$  SD.

**Figure 7** – Flow Cytofluorimetric evaluation of blood, spleen and bone marrow (n = 5 randomly chosen mice per group). Total leukocyte count in the blood of EKO (A) and WT (D); count of T and B cells, monocytes and neutrophils in the blood of EKO (B) and WT (E); percentage of activated (Ly6C<sup>hi</sup>) and resting monocytes (Ly6C<sup>lo</sup>) in the blood of EKO (C) and WT (F). Total count of leukocytes in the femur of EKO and WT mice (G); percentage of myeloid precursors (CD11b<sup>+</sup>) on total leukocytes (H) and their subsets (J, L), representative dot plot from FACS analysis are shown (I);



Immature (Ly6G<sup>hi</sup>) and mature (Ly6G<sup>lo</sup>) monocyte progenitors in EKO (K) and WT (M) bone marrow. Total count of spleen's immune cells in EKO (N, P) and WT (O, Q); cell count corrected for spleen weight (mg) in EKO (R, T) and WT (S, U). GMP: granulocyte/monocyte progenitors; GP: granulocyte progenitors; MP: monocyte progenitors. Statistically significant differences were determined by unpaired two-tailed Student's T-test. \*:  $p < 0.05$ ; \*\*:  $p < 0.01$ ; \*\*\*:  $p < 0.001$ . Data are expressed as mean  $\pm$  SD.

**Figure 8** – Spleen (H&E, **A,B**); extramedullary hematopoiesis expanding the red pulp mostly represented by erythroid cells: mild in EKO-Ctrl (**A**) with a large follicle on the right and severe in EKO-Fen (**B**) with an atrophic follicle on the right. Liver (H&E, **C,D**); extramedullary hematopoiesis: negative in EKO-Ctrl (**C**) and moderate in EKO-Fen expanding a portal area (**D**). Liver (Perls' iron stain, **E,F**); hemosiderin in the cytoplasm of Kupffer cells: negative in EKO-Ctrl (**E**) and moderate, multifocal presence in EKO-Fen (**F**). Kidney (H&E, **G,H**); hemosiderin, represented by granular brownish material, in the cytoplasm of proximal convoluted tubular epithelial cells: negative in EKO-Ctrl (**G**) and severe, multifocal presence in EKO-Fen (**H**). Kidney (Perls' iron stain, **I,J**); hemosiderin, represented by blue granules, in the cytoplasm of proximal convoluted tubular epithelial cells: negative in EKO-Ctrl (**I**) and severe, multifocal presence in EKO-fen (**J**). Bar length: 100  $\mu$ m.

**Figure 9:** Flow cytometry analyses of percentage of (**A**) monocyte & neutrophil - platelet and (**B**) monocyte - platelet aggregates in whole blood of WT and EKO mice treated with or without fenretinide ( $n = 5$  randomly chosen mice per group). In **A**, aggregates in EKO-Ctrl were higher than both untreated groups ( $p = 0.001$  and  $p = 7.96 \times 10^{-5}$  vs WT and EKO, respectively), as well as aggregates in EKO-Fen were higher than both untreated groups ( $p = 0.004$  and  $p = 2.5 \times 10^{-4}$  vs WT and EKO, respectively). In **B**, aggregates in WT-Fen were different from all EKO conditions ( $p = 0.0128$  and  $p = 1.3 \times 10^{-5}$  vs EKO untreated and treated, respectively). Fenretinide treatment resulted in significantly different aggregates in EKO ( $p = 0.0017$  in EKO-Ctrl vs EKO-Fen). Statistically significant differences were determined by Kruskal-Wallis one-way analysis of variance test, followed by Conover's post-hoc test with Bonferroni  $p$ -value adjustment method. Top: the upper and lower ends of the boxes

indicate the 25<sup>th</sup> and 75<sup>th</sup> percentiles, respectively. The length of the box shows the interquartile range within which 50% of the values are located. The solid gray lines denote the median. Bottom: data are expressed as mean  $\pm$  SD.

For Peer Review

Figure 1

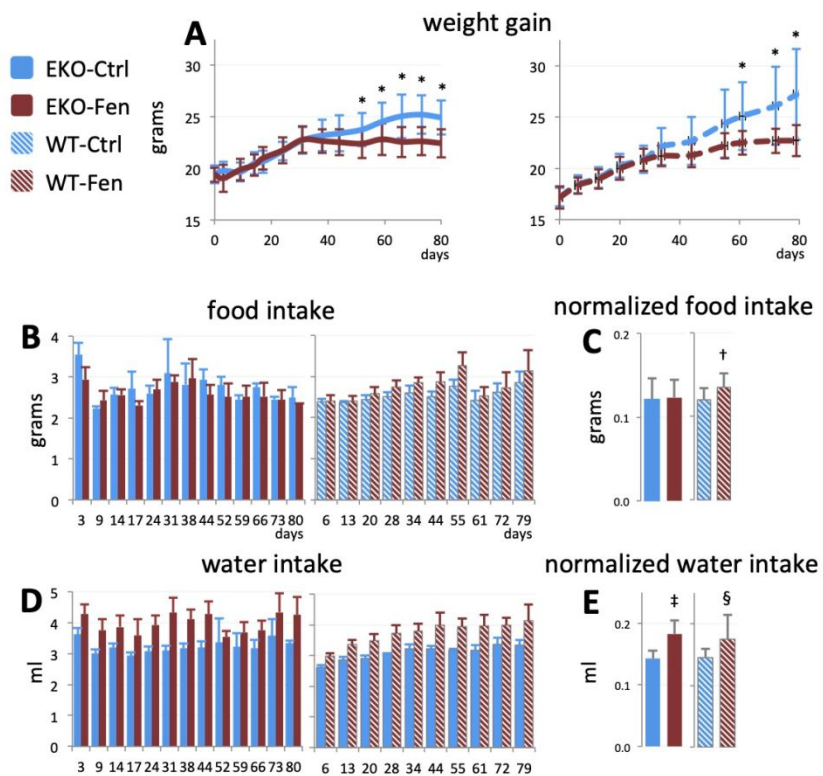
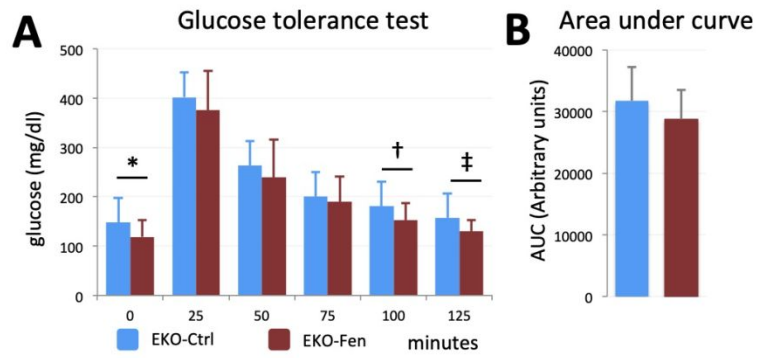


Figure 2



Review

Figure 3

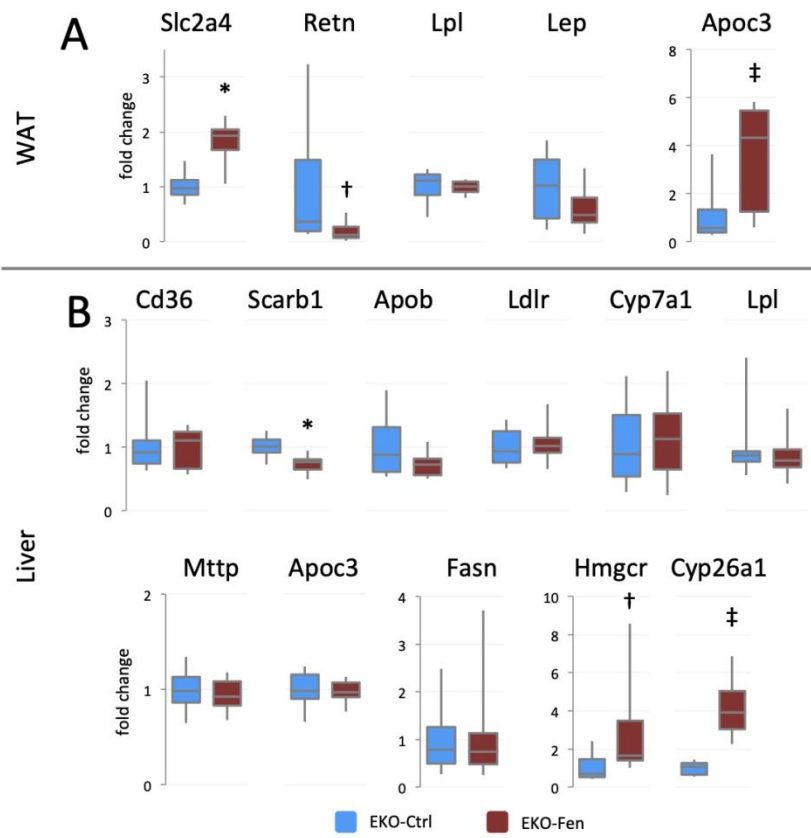


Figure 4

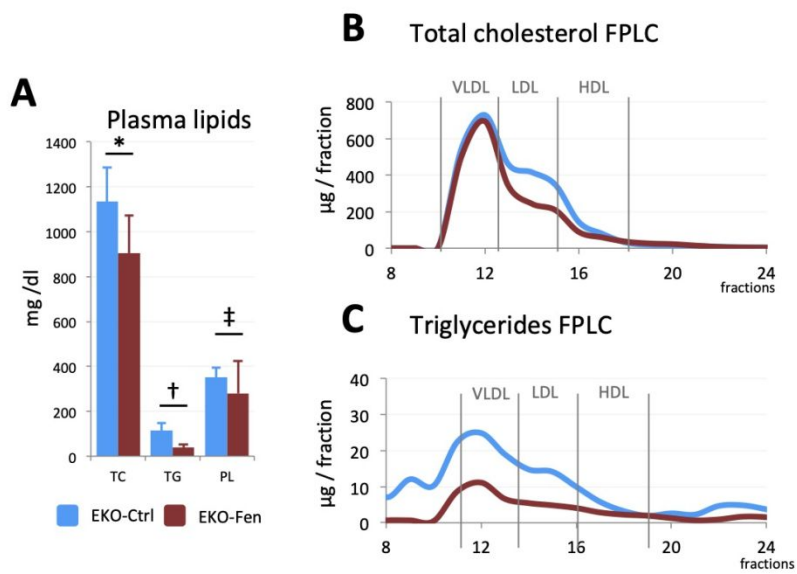


Figure 5

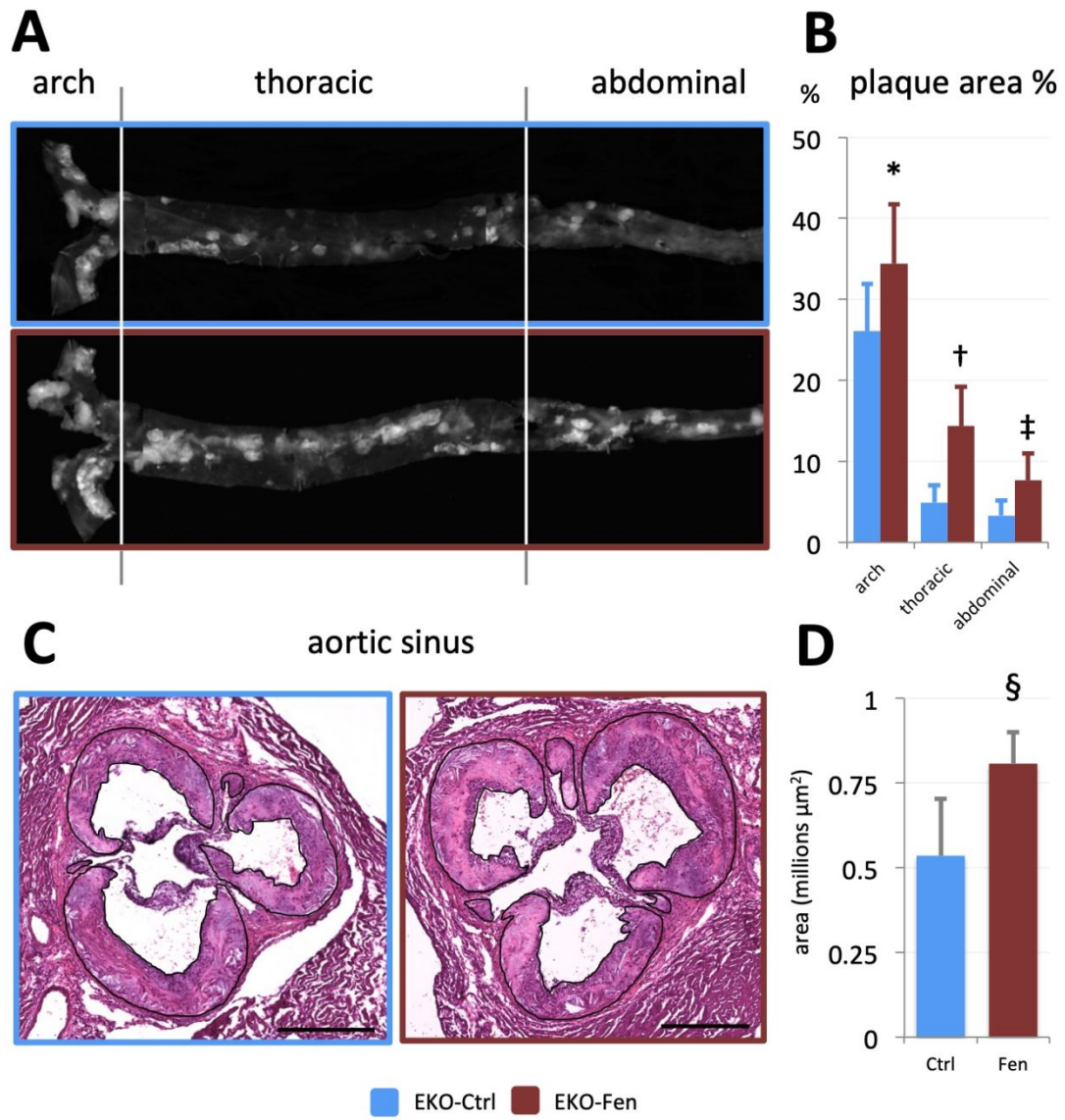


Figure 6

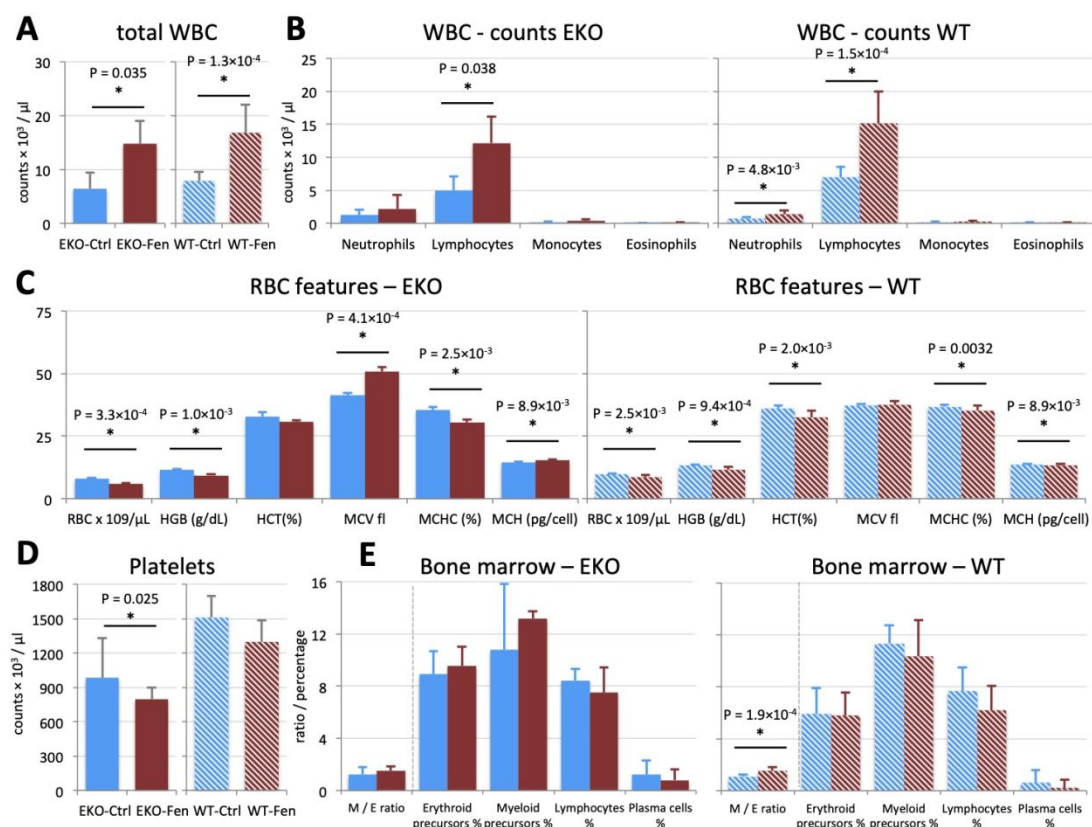




Figure 7

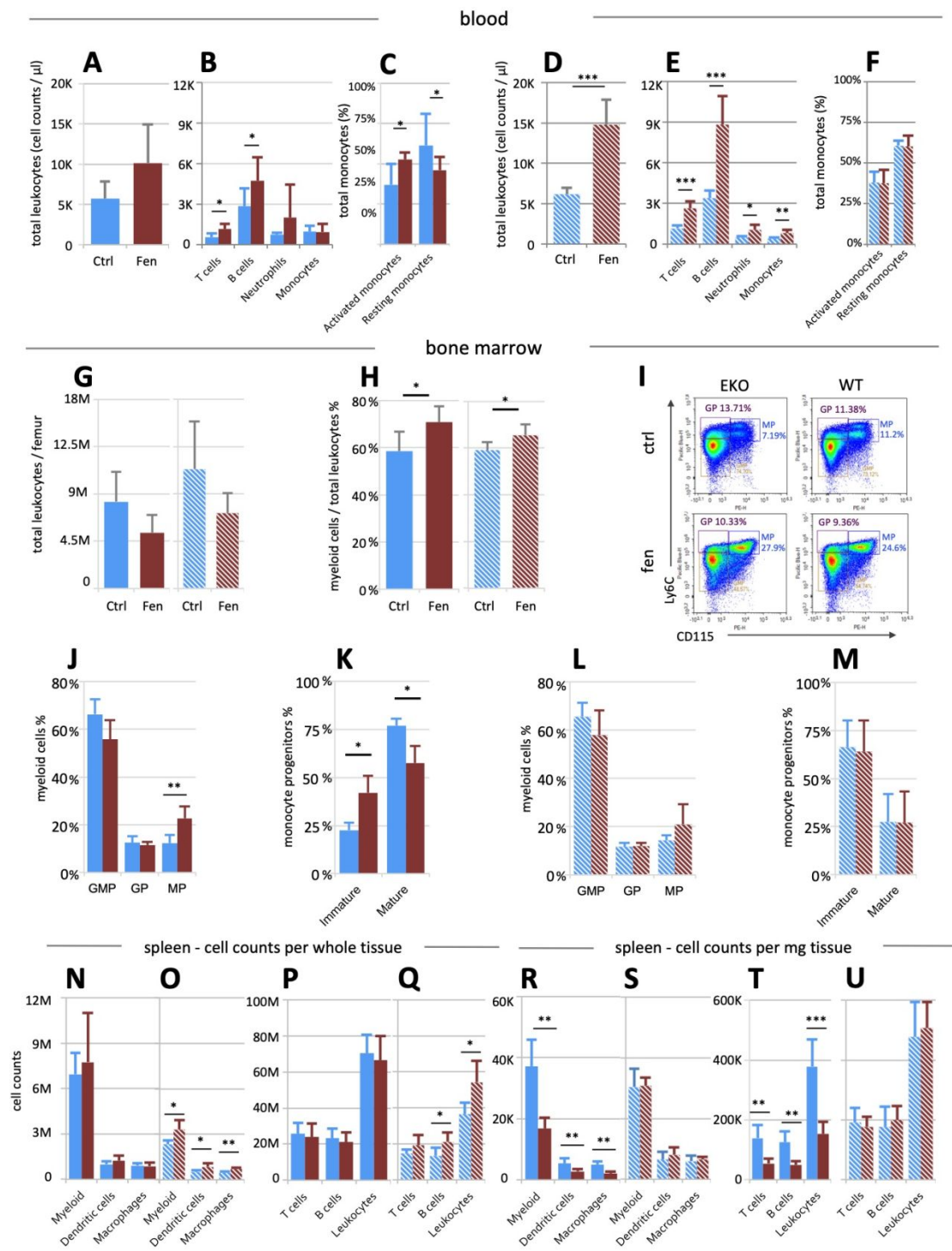


Figure 8

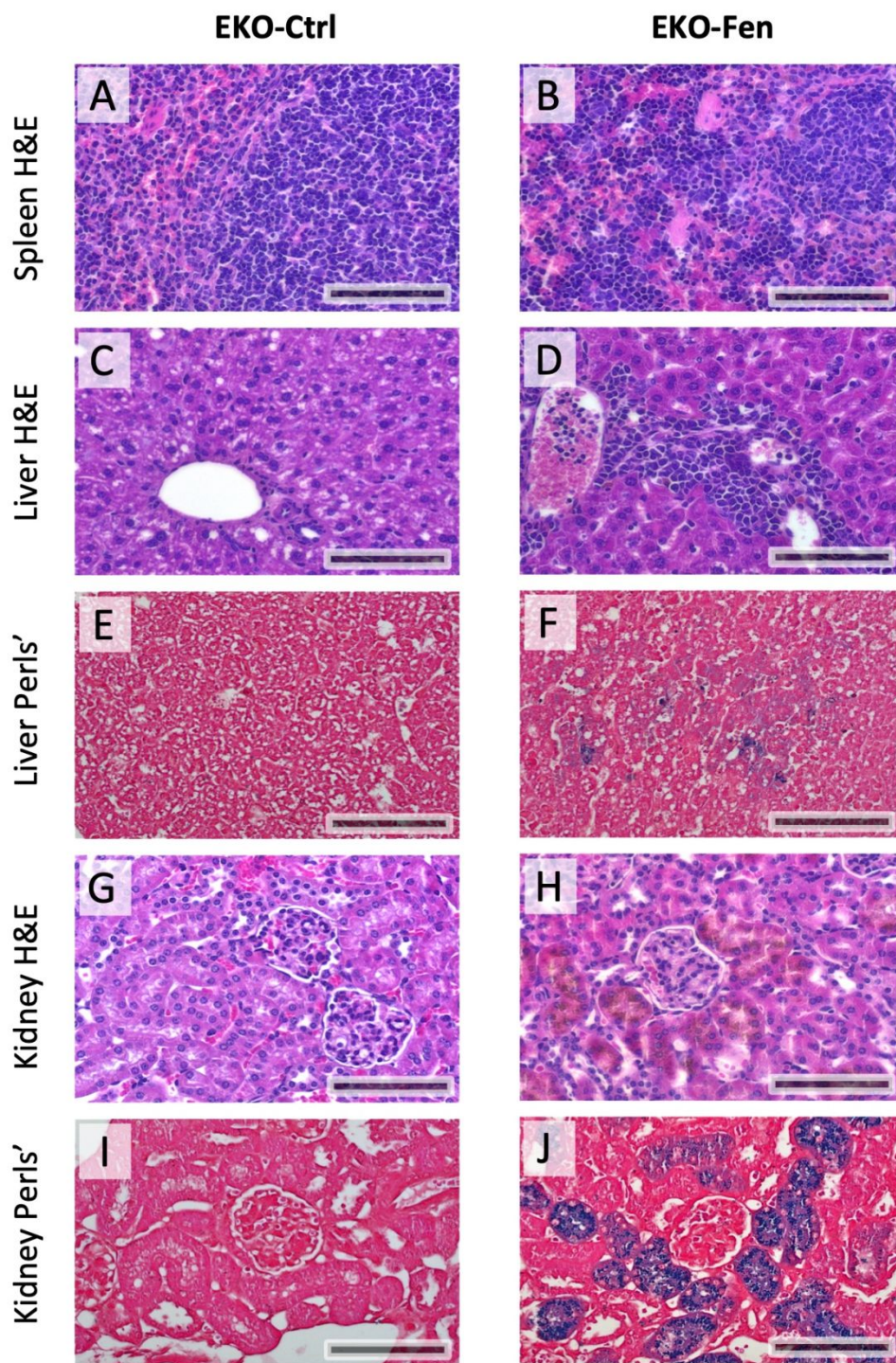
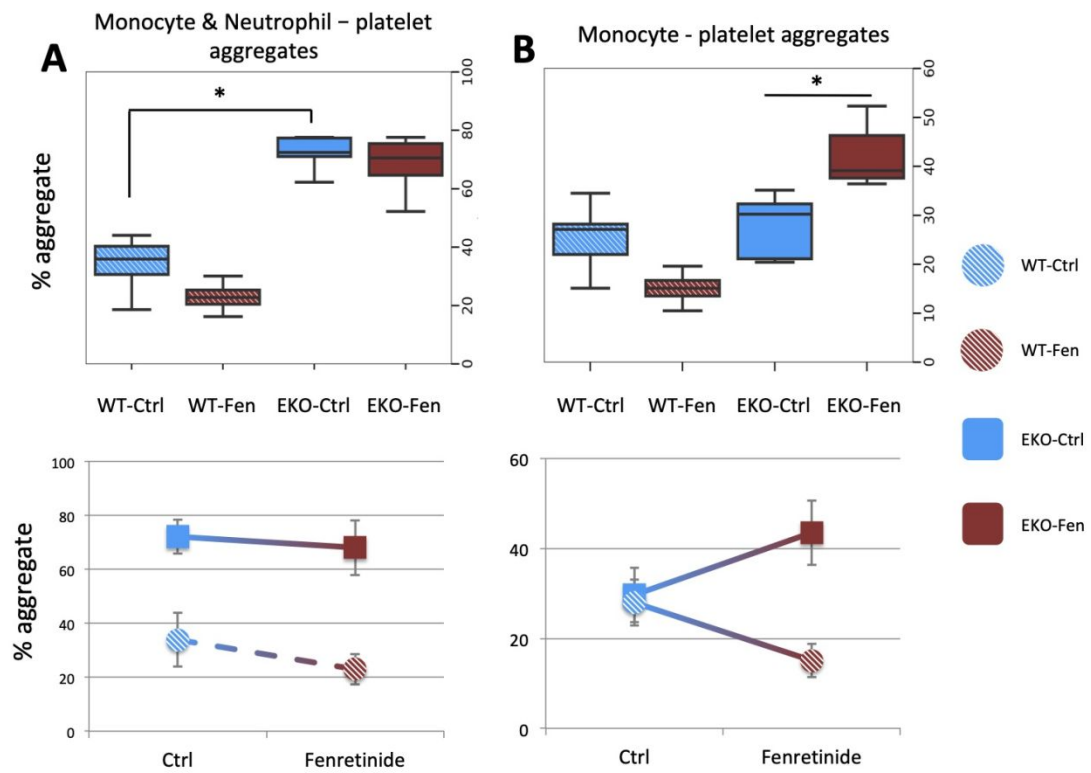
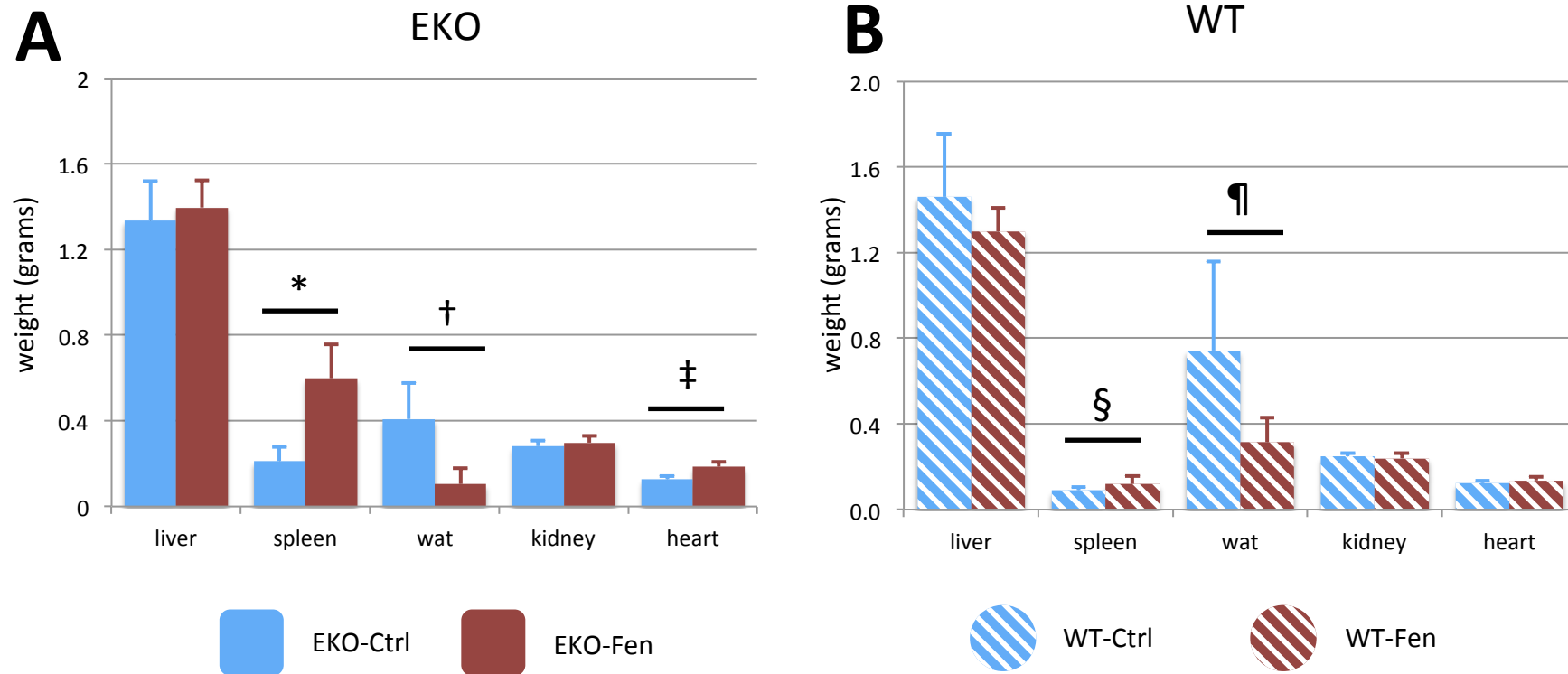


Figure 9



Review

## Supplementary Figure 1



Weight of organs sampled at sacrifice in WT (**A**) and EKO (**B**) mice (EKO: n = 20; WT: n = 10). \*  $p = 7.8 \times 10^{-12}$ ; †  $p = 2.8 \times 10^{-8}$ ; ‡  $p = 1.9 \times 10^{-10}$ ; §  $p = 0.035$ ; ¶  $p = 0.0056$ . Statistically significant differences were determined by unpaired two-tailed Student's T-test. Data are expressed as mean  $\pm$  SD.



## Supplementary Figure 2

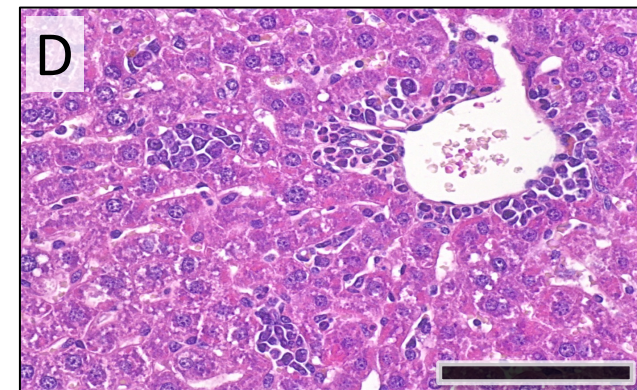
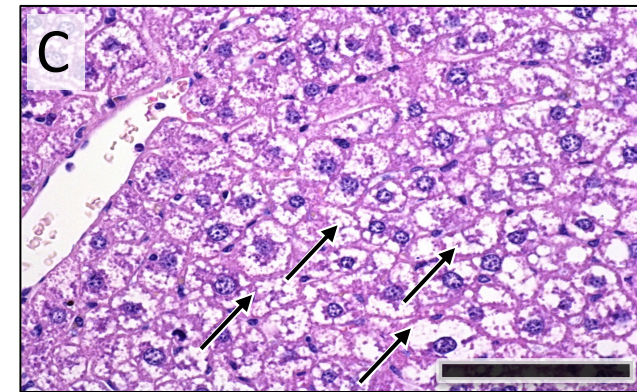
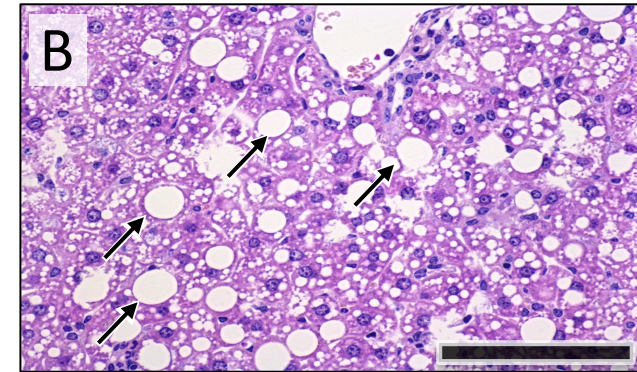
## A Liver histological features

Table LIVER - Liver histological features

	Glycogen		Steatosis		Hematopoiesis
	Severity	Distribution	Severity	Distribution	
EKO-Ctrl	+++	D	++	R	-
	++	P	+	P	-
	++	D	+	P	+
	+	D	+	R	-
	++	D	-	\	-
	-	\	+++	R	-
	++	D	+	R	-
	+++	D	-	\	-
	+++	D	+	P	-
	+++	D	+	P	-
EKO-Fen	-	\	-	\	+
	+	D	-	\	+
	+	D	-	\	+
	-	\	+	R	+
	-	\	-	\	+
	-	\	-	\	++
	-	\	-	\	++
	-	\	-	\	+
-	\	+	R	++	
+	D	-	\	+	

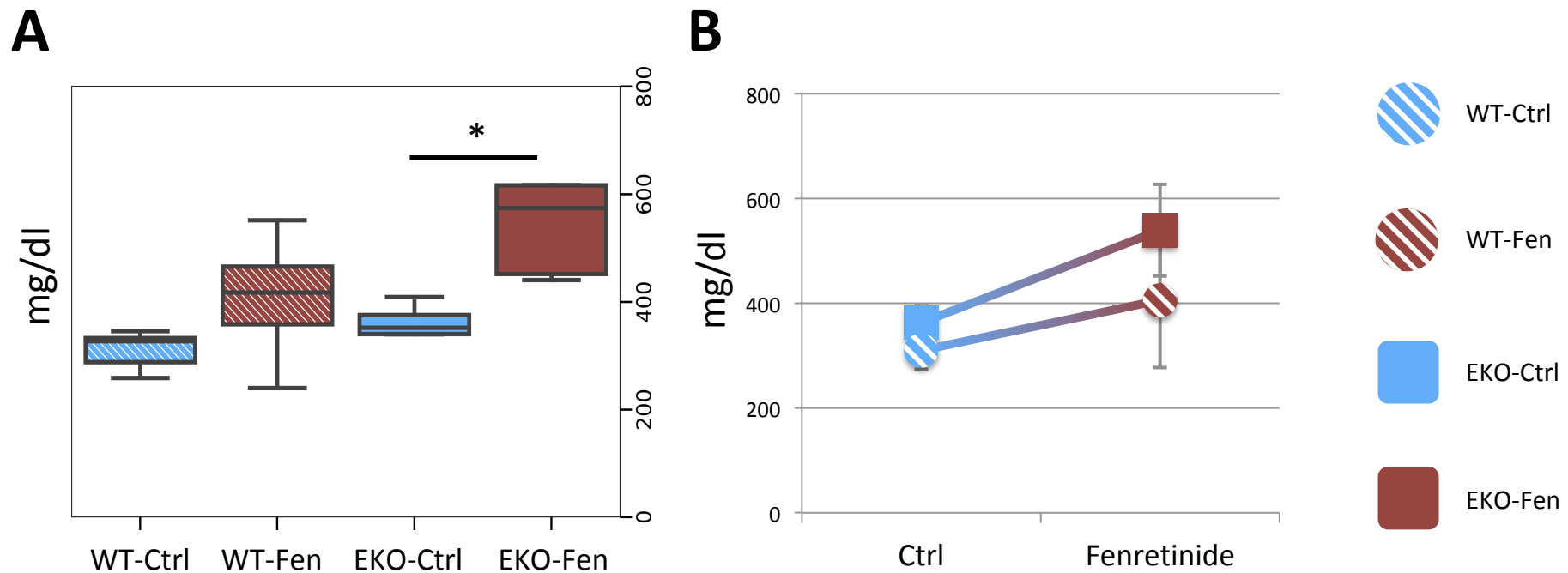
p=5.1×10<sup>-4</sup>

p=0.0041

p=6.7×10<sup>-4</sup>

**A:** In the liver of EKO mice, glycogen accumulation and steatosis were given an arbitrary score, either - (absent), + (slight), ++ (moderate) or +++ (severe). Their distribution was also ranked as Diffuse = D; Centrolobular = C; Periportal = P; Random = R. **B:** representative H&E image of liver steatosis (arrows) in EKO-Ctrl. **C:** representative H&E image of hepatic glycogen accumulation (arrows) in EKO-Ctrl. **D:** representative H&E image of hepatic tissue devoid of steatosis and glycogen accumulation in EKO-Fen. Features were evaluated by an operator blinded to experimental groups. Statistically significant differences were determined by unpaired two-tailed Mann-Whitney U test. n = 10, randomly chosen. Bar length: 100 μm.

## Supplementary Figure 3

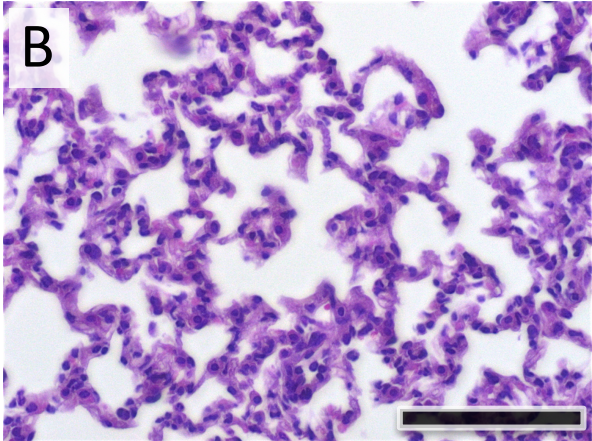


Functional fibrinogen concentration in plasma is shown (n = 5 randomly chosen mice per group), \* p= 0.0371. Statistically significant differences were determined by Kruskal-Wallis one-way analysis of variance test, followed by Conover's post-hoc test with Bonferroni p-value adjustment method. Left: the upper and lower ends of the boxes indicate the 25<sup>th</sup> and 75<sup>th</sup> percentiles, respectively. The length of the box shows the interquartile range within which 50% of the values are located. The solid gray lines denote the median. Right: data are expressed as mean  $\pm$  SD.

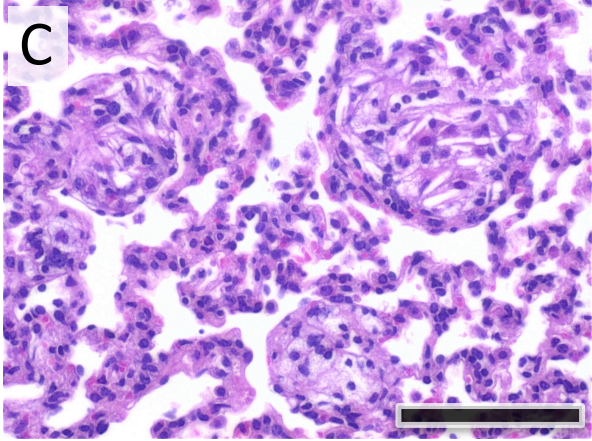


## Supplementary Figure 5

A	Perivascular/peribronchial inflammatory infiltrates		Foamy macrophages		Cholesterol crystals
	severity	cell type	single cells	group of cells	
EKO-Ctrl	-	\	-	-	-
	+	L	-	-	-
	-	\	-	-	-
	+	L	-	-	-
	-	\	-	-	-
	-	\	-	-	-
	+	L	-	-	-
	-	\	-	-	-
	-	\	-	-	-
	-	\	-	-	-
EKO-Fen	++	L	+++	++	+
	+	L, P	+	+	-
	-	\	+	-	-
	-	\	-	+	+
	+	L	+	+++	-
	-	\	++	+++	-
	-	\	+	++	-
	-	\	++	++	-
	+	L	++	+++	++
	+	L	++	++	-
	p=NS		p=1.0×10 <sup>-4</sup>	p=1.0×10 <sup>-4</sup>	p=0.038



**B**

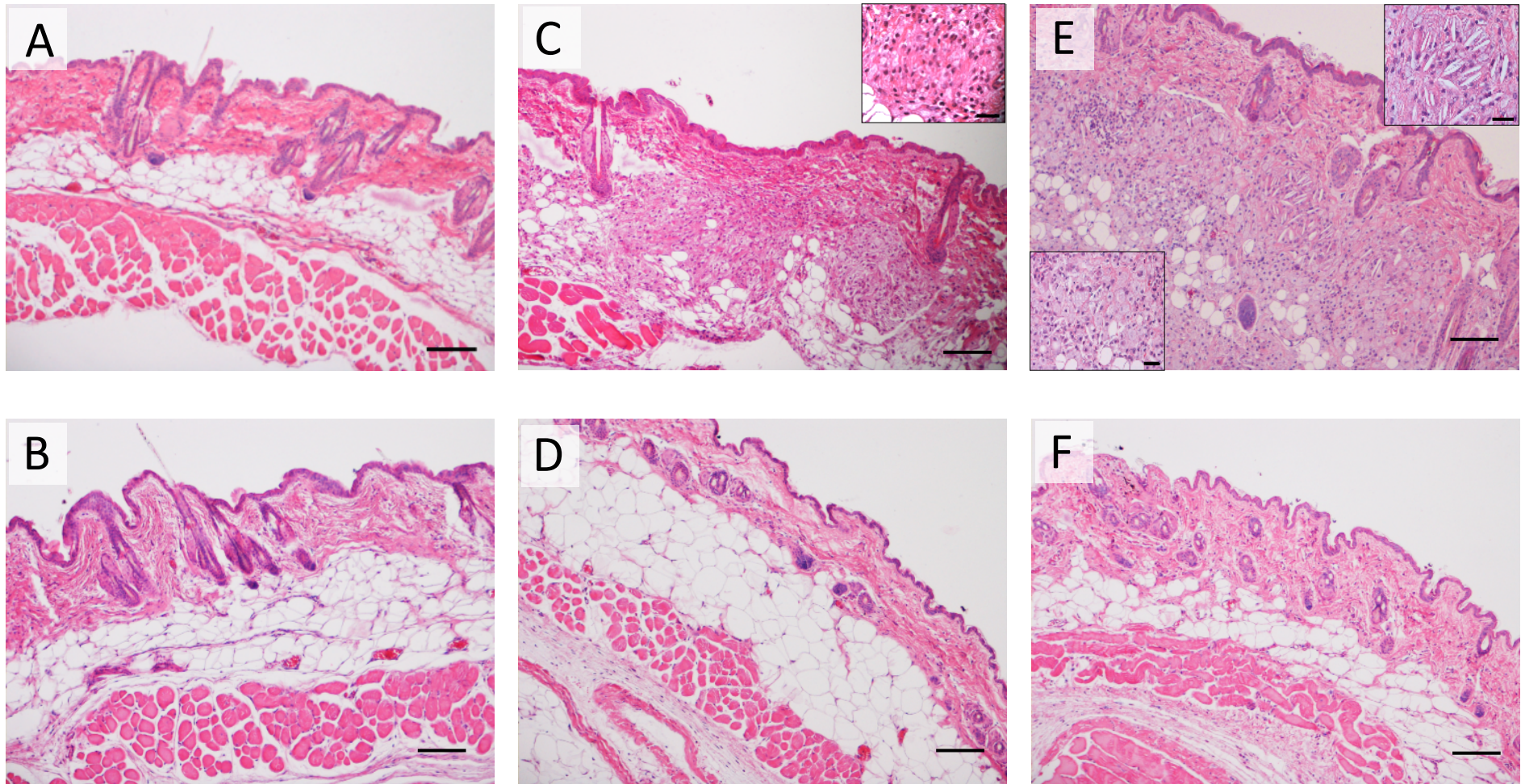


**C**

**A.** In the lung, inflammatory infiltrates were evaluated and ranked as follows: - (no infiltrate), + (rare, < 3 infiltrates), ++ (some, 3 - 5 infiltrates) and +++ (numerous, > 5 infiltrates). Cell types found were labelled L (lymphocytes) and/or P (plasma cells). Foamy macrophages were counted per field, and ranked as follows: - (absent), + (rare, < 5), ++ (few, 5 - 15), +++ (numerous, > 15). Cholesterol crystals were similarly ranked from none (-) to abundant (+++). Features were evaluated by an operator blinded to experimental groups. Statistically significant differences were determined by unpaired two-tailed Mann-Whitney U test. 10 random samples from EKO-Fen and EKO-Ctrl groups were chosen for analyses. **B,C:** representative photomicrographs of H&E stained EKO-Ctrl and EKO-Fen, respectively. Bar length: 100  $\mu$ m.



## Supplementary Figure 6



Representative H&E photomicrographs of mouse skin sections. **A**: WT-Ctrl; **B** WT-Fen; **C** and **D**: EKO-Ctrl; **E** and **F**: EKO-Fen. Foam cells accumulation is shown in C, top-right and E, bottom-left. Cholesterol clefts accumulation in the dermis is shown in E, top-right.

Bars: A-F: 60  $\mu$ m; small boxes: 15  $\mu$ m.

Supplementary Table 1

Gene ID	Forward Primer 5' → 3'	Reverse Primer 5' → 3'	Amplicon size	Organ(s)
Apob	AGCGCCACCAAGATCAACTG	GTTTCGTACCTGGACATGGCA	178	liver
Cd36	GGTGGATGGTTTCCTAGCCTT	GTGGCCCGTTCTACTAATTCAT	135	liver
Cyp26a1	CCGTGAGAAGCTGCAGTGTA	GGGTTCCATCCTTCAGCTCC	119	liver
Cyp7a1	AACAACCTGCCAGTACTAGATAGC	GTGTAGAGTGAAGTCCTCCTTAGC	99	liver
Fasn	GGAGGTGGTGATAGCCGGTAT	TGGGTAATCCATAGAGCCCAG	140	liver
Hmgcr1	AGCCGAAGCAGCACATGAT	GGGTATTGCTGGCCTCTCA	215	liver
Ldlr	TCGTAGTGGACCTGTGCAT	GGAAAGATCTAGTGTGATGCCATT	149	liver
Mtp	AGCGTGGTGAAAGGGCTTAT	CCACAGCCACCCGATTTTTTC	178	liver
Scarb1	ATGGGCCAGCGTGCTTTTATGAAC	ACGCCCCTGAAGACAGTGAAGACC	179	liver
Apoc3	CATCTGCCCGAGCTGAAGA	GCTTGTTCCATGTAGCCCTGTAC	70	liver, WAT
Lpl	GGGAGTTTGGCTCCAGAGTTT	TGTGTCTTCAGGGGTCCTTAG	115	liver, WAT
Pck2	GGAGCACAAGGAAAGACCA	GACATGGAAGATACGAGGCAG	139	liver, WAT
Ppia	AGCACTGGGGAGAAAGGATT	AGCCACTCAGTCTTGGCAGT	248	liver, WAT
Lep	AGCAGTGCCTATCCAGAAAGTCCA	AATGAAGTCCAAGCCAGTGACCCT	127	WAT
Retn	CCTACACACTCAGCAGTACGGAC	TCAAACCTCTGTATAGAACTTGCGGA	157	WAT
Slc2a4	CTGTGCCATCTTGATGACCGTG	GTTGGAGAAACCAGCGACAGC	196	WAT

Cycling conditions were as follows: initial denaturation for 1' at 95 °C, followed by 40 cycles of 10s at 95°C and 30s at 60 °C. After the run, a melting curve was performed (0.5 °C increases over 5 seconds, from 65 °C to 95 °C). Cqs equal or higher than 35 were excluded from the analysis and primer pairs calibration.

**Supplementary Table 2 - Spleen histological features**

	Hematopoiesis	Follicular atrophy	Foamy macrophages
EKO-Ctrl	+	-	-
	++	-	-
	++	-	-
	+	-	-
	+	-	+
	+++	+++	-
	+	-	-
	+	-	-
	+	-	-
	+	-	-
EKO-Fen	+++	+++	+
	+++	+++	-
	+++	++	-
	++	++	-
	+++	++	-
	+++	++	++
	++	+	-
	++	+	-
	+++	+	-
	++	+	-
	p=0.002	p=0.001	p=NS

In the spleen, hematopoiesis and follicular atrophy features were evaluated and ranked as follows: - (absent), + (slight), ++ (mild) and +++ (severe). Foamy macrophages were counted per area, and ranked as follows: - (absent), + (rare), ++ (few), +++ (numerous). Features were evaluated by an operator blinded to experimental groups. Statistically significant differences were determined by unpaired two-tailed Mann-Whitney U test. 10 random samples from EKO-Fen and EKO-Ctrl groups were chosen for analyses.

**Supplementary Table 3 - Kidney histological features**

	<b>Glomerular lipidosis</b>	<b>Tubular pigment deposition</b>
EKO-Ctrl	++	-
	++	-
	+	-
	+++	-
	+++	-
	++	-
	++	-
	+	-
	+	-
	++	-
<hr/>		
EKO-Fen	+++	+++
	++	++
	++	++
	++	+
	+	+++
	+	++
	+	+
	-	++
	++	+++
	+	++
	p=NS	p=2.8×10 <sup>-5</sup>

In the kidney, pigment deposition was evaluated and ranked as follows: - (absent), + (slight), ++ (mild) and +++ (severe). Features were evaluated by an operator blinded to experimental groups. Statistically significant differences were determined by unpaired two-tailed Mann-Whitney U test. 10 random samples from EKO-Fen and EKO-Ctrl groups were chosen for analyses.

Supplementary Table 4 - Skin morphology

		Foam cells	Crystals	Mast cells	Lymphocytes
WT	Ctrl	-	-	+	-
		-	-	+	-
		-	-	+	-
		-	-	+	-
		-	-	+	-
	Fen	-	-	+	-
		-	-	+	-
		-	-	-	-
		-	-	+	-
		-	-	++	-
		p=NS	p=NS	p=NS	p=NS
EKO	Ctrl	+	-	++	-
		+	-	-	-
		+++	+	-	-
		++	-	++	-
		+	-	+	-
	Fen	+++	++	-	+
		+++	+++	-	+
		+	-	++	-
		-	-	+	-
		+	-	+	-
		p=NS	p=NS	p=NS	p=NS
WT vs EKO					
		p=0.000113	P=0.05054	p=NS	p=NS

In the skin, foam cells, mast cells, lymphocytes and the presence of cholesterol crystals were evaluated and ranked as follows: - (no infiltrate), + (rare), ++ (some) and +++ (numerous). Features were evaluated by an operator blinded to experimental groups. Statistically significant differences were determined by unpaired two-tailed Mann-Whitney U test. 5 random samples from WT-Ctrl, WT-Fen, EKO-Ctrl and EKO-Fen groups were chosen for analyses.

Supplementary Table 5 - Wild-type histological features

	Kidney				Liver						Spleen	Lungs		
	Ialine cast	Lymphocytic interstitial infiltrate	Hypercellular glomeruli	Tubular Pigment Deposition	Glycogen	Steatosis	Pigment deposition	Inflammatory infiltrate number	Infiltrate size (S<10; M<100; L>100)	perivascular Inflammatory infiltrate number	Infiltrate size (S<10; M<100; L>100)	Hematopoiesis	single cells	group of cells
WT-Ctrl	+	-	-	-	++	-	-	2	M	0	-	+	-	-
	-	++	-	-	+	-	-	1	S	1	S	+	-	-
	-	-	-	-	++	-	-	1	S	1	S	-	-	-
	-	-	-	-	++	-	-	0	-	0	-	-	-	-
	+	-	-	-	++	-	-	0	-	0	-	+	-	-
	+	-	-	-	+++	-	-	0	-	0	-	+	-	-
	-	-	-	-	+	-	-	3	S	0	-	-	-	-
	+	-	-	-	++	-	-	3	S	1	S	-	-	-
	+	-	-	-	+	-	-	3	S	1	S	-	-	-
	+	-	-	-	+++	-	-	0	-	0	-	-	-	-
WT-Fen	+	-	-	-	+	-	-	1	S	0	-	+	-	-
	++	-	-	-	+	-	-	2	S	0	-	+++	-	-
	++	-	-	-	+	-	-	1	M	0	-	+	-	-
	++	-	-	-	+	-	-	3	S	0	-	+	-	-
	+	-	-	-	+	-	-	1	S	1	M	-	-	-
	-	-	-	-	+	-	-	7	S	1	M	-	-	-
	-	-	-	-	++	-	-	1	M	0	-	+	-	-
	+	-	-	-	++	-	-	4	S	0	-	+	-	-
	-	-	-	-	+	-	-	3	S	2	M	+	-	-
	-	-	+	-	+	-	-	0	-	0	-	+	-	-
	p = NS	p = NS	p = NS	p = NS	p = 0.024	p = NS	p = NS	p = NS	p = NS	p = NS	p = NS	p = 0.064	p = NS	p = NS

Histological features (n=10 per group) were scored as follows: Kidney: Ialine casts = Ialine intratubular (medullary) cast: 1-3 = +; 4-10 = ++; < 10 = +++; Grading of other findings: - = absent; + = slight; ++ = moderate; +++ = severe; Liver: grading of findings: - = absent; + = slight; ++ = moderate; +++ = severe; S = small (up to 10 cells); M = medium (11-100 cells); Spleen, Lungs: Grading of findings: - = absent; + = slight; ++ = moderate; +++ = severe. For ranked data, statistically significant differences were determined by unpaired two-tailed Mann-Whitney U test. For numerical data, statistically significant differences were determined by unpaired two-tailed Student's T-test.